ESA CONTRACT REPORT

Contract Report to the European Space Agency

TNPII WP3401 & WP3402 SMOS Report on background and observation error scenarios

Joaquín Muñoz Sabater, Patricia de Rosnay, Clément Albergel, Lars Isaksen

ESA/ESRIN Contract 4000101703/10/NL/FF/fk

European Centre for Medium-Range Weather Forecasts
Europäisches Zentrum für mittelfristige Wettervorhersage
Centre européen pour les prévisions météorologiques à moyen terme

ECMWF

Series: ECMWF ESA Project Report Series

A full list of ECMWF Publications can be found on our web site under:
http://www.ecmwf.int/en/research/publications

Contact: library@ecmwf.int

European Centre for Medium Range Weather Forecasts
Shinfield Park, Reading, RG2 9AX, England

Contract Report to the European Space Agency

TNPII WP3401 & WP3402
SMOS Report on background and observation error scenarios

Authors: Joaquín Muñoz Sabater,
Patricia de Rosnay,
Clément Albergel,
Lars Isaksen
ESA/ESRIN Contract 4000101703/10/NL/FF/fk

European Centre for Medium-Range Weather Forecasts
Shinfield Park, Reading, Berkshire, UK

January 2016

	Name	Company
First version prepared by (October 2014)		ECMWF
Quality Visa		ECMWF
Application Authorized by		ESA/ESRIN

Distribution list:

ESA/ESRIN
Susanne Mecklenburg
ESA ESRIN Documentation Desk

SERCO
Raffaele Crapolicchio

ESA/ESTEC
Matthias Drusch

ECMWF
DR
Division & Section Heads

Contents

1 Introduction

For short, medium and extended range weather predictions, soil moisture is (in snow-free surfaces) a very important variable. The reason is the strong influence that it has in the energy, water and carbon fluxes, and thus accurate analyses of soil moisture in Numerical Weather Prediction systems are important. The last decade has accrued a large number of studies using data assimilation systems to constrain soil moisture with the available observations. An important component of these systems is their ability to incorporate not only the information from independent observations to the model, but also the associated uncertainty. By assigning correct weights to observations and model background, they are able to produce an optimal estimate of the soil moisture state (which is generally of superior quality to only model based estimations). It is difficult to assign errors to observations and model background which accurately represent all the known sources of uncertainties (e.g., instrumental, algorithm, model parameterisation, atmospheric forcing and representativeness). This is not a straightforward task and indeed there is very little knowledge on the correct specification of these errors in data assimilation systems. However, analyses are very sensitive to this information.

In this study the ECMWF Simplified Extended Kalman Filter (SEKF) (Drusch et al. 2009; de Rosnay et al. 2012) is used. A soil moisture background value is corrected by accounting for the difference between observations and model equivalents. This difference is modulated by the gain of the Kalman filter, that depends on observations and background errors. This report tests different scenarios for the observation and background error covariance matrices in the ECMWF SEKF. The variables analysed are soil moisture of the top three layers of the Hydrology-Tiled ECMWF Scheme for Surface Exchange over Land (H-TESSEL) (Balsamo et al. 2009). The soil moisture background value is adjusted by assimilating 2 m temperature and 2 m relative humidity observations (as proxies for soil moisture), and brightness temperatures (Muñoz-Sabater et al. 2012; Muñoz-Sabater et al. 2014) from the Soil Moisture and Ocean Salinity (SMOS) mission of the European Space Agency (ESA). The background error information injected in the SEKF is currently constant. Likewise, screen level observation errors are also constant, whereas for SMOS observations the pure radiometric accuracy, individual to each observation, is used as observation error. The main goal of this study is to investigate the sensitivity of soil moisture analyses to different background and SMOS brightness temperatures error scenarios in the ECMWF SEKF. A range of data assimilation experiments using different approaches (pseudo-direct insertion or simplified Extended Kalman Filter [EKF]), with SMOS data combined or not with other types of observations, were conducted. Different configurations of the SMOS observation error (increasing or decreasing the confidence in the observations) and model background error representation (static or propagated in time, with or without soil texture dependence) were investigated. Results of these experiments were compared against in-situ data from the USCRN and SCAN networks in USA. In addition to the land hydrological aspects, the atmospheric impact on meteorological variables was also evaluated.

2 Methodology

2.1 The ECMWF soil moisture analysis and errors definition

The ECMWF soil moisture analysis is able to combine screen level observations (2 m temperature and 2 m relative humidity) and satellite observations (currently there are capabilities implemented to assimilate ASCAT and SMOS data) with model soil moisture, to produce a soil moisture analysis at time t_i:

$$\mathbf{sm}^a(t_i) = \mathbf{sm}^b(t_i) + \mathbf{K}_i[\mathbf{y}^o(t_i) - H_i(\mathbf{x}^b)]$$

with superscripts a, b, o standing for background, analysis and observations, respectively. In this eq, $\mathbf{y}$ is the observation vector and H is the non-linear observation operator, which transform the background from model space to observation space for comparison. The state vector **sm** consists of the soil moisture of the top three layers of the ECMWF land surface model H-TESSEL. In this study, the term of most interest is the Kalman gain matrix $\mathbf{K}_i$, computed at time t_i as:

$$\mathbf{K}_i = [\mathbf{B}^{-1} + \mathbf{H}_i^T\mathbf{R}^{-1}\mathbf{H}_i]^{-1}\mathbf{H}_i^T\mathbf{R}^{-1}$$

The linearised observation operator $\mathbf{H}_i$ is numerically obtained by finite differences, whereas $\mathbf{B}$ is the error covariance matrix associated to the background soil moisture state and $\mathbf{R}$ is the observation error covariance matrix. In a Kalman Filter, the background error covariance matrix evolves between time i and $i+1$ according to:

$$\mathbf{B}_{i+1} = \mathbf{M}\mathbf{B}_i\mathbf{M}^T + \mathbf{Q}$$

where $\mathbf{M}$ is the prognostic model operator, and $\mathbf{Q}$ is the model error covariance matrix.

Currently it is assumed that the background error covariance of the state variables is constant during the whole assimilation period, and with a value equal to $0.01 m^3 m^{-3}$ for each model soil layer. This approach is rather conservative and assumes that the model soil moisture of the top three layers are affected by the same errors. However, the top layer is affected by larger variability, especially after raining events, leading to a likely larger error that the relatively more stable temporal evolution of soil moisture in deeper layers. Soil texture is a very important parameter in accurate soil moisture modeling. None of these two factors are accounted for in the current definition of background errors. In this study, these two factors are taken into account to set different scenarios for the background error as described in section 2.2. On the observation side, the screen temperature and relative humidity covariance error is also fix and calibrated to 2 K and 10%, respectively. These values have been recently revised and they were replaced by 1 K and 4% in the ECMWF operational cycle cy41r1. Each SMOS multi-angular, multi-polarised observation, has been assigned an unique observation error which is related to the radiometric accuracy. However, this approach likely confers too much weight to the SMOS observations, as it does not account for other sources of instrumental errors and of representativity of the soil depth at which is sensitive. Based on these shortcomings in the specification of model and observation errors, in this study different scenarios are tested and described in the next section.

2.2 Experiment types

A series of 1-month assimilation experiments at T511 spectral resolution (approximately 40 km horizontal spatial resolution) were run over the US, to test the impact of different observation and model error scenarios

on soil moisture and atmospheric variables. The period of integration spans from 15 September 2012 to 14 October 2012. This is a period of hydrological recharge in the US, where strong variability of soil moisture was recorded. In these experiments, SMOS observations were assimilated at incidences angles of 30, 40 and 50 degrees, and at pure XX and YY polarisations, respectively. Only the Alias Free Field-Of-View (FOV) was considered, as being the area of the FOV delivering data of highest quality. Likewise, SMOS flags of the Near Real Time (NRT) product were used to filter data affected by Radio Frequency Interference (RFI). The physical parameterisations of ECMWF cy40r1 were used in these experiments. The upper-air atmospheric analysis is based on the 12-hours 4DVAR system. However, in order to reduce the computational cost of these experiments and to better observe the impact produced by these experiments, only in-situ observations and satellite data from the Advanced Television and Infra-red Observational Satellite (ATOVS), Ground Based Radar precipitation data (GBRAD) and Next-Generation Radar (NEXRAD), were used to constrain the atmospheric integrations. The consequence of using such a reduced observational system is the lost of accuracy of the spatial-temporal evolution of the atmospheric variables, whereas it is assumed that the impact on surface variables is small for the area and period under study.

The following experiments were defined:

(i) **OL**: This is the control experiment, running in open-loop configuration where the soil moisture state is obtained by a free run of the land surface model without any additional update, i.e., no soil moisture analysis is performed;

(ii) **SLV**: Screen-level variables assimilation only, which updates the soil moisture state based on indirect information provided by in-situ observations of 2m temperature and 2m relative humidity. It uses the same configuration as the operational soil moisture analyses, but at reduced spatial resolution;

(iii) **SLV+SMOS**: Combined assimilation of screen-level variables and SMOS brightness temperatures with observation and background errors as defined in section 2.1;

(iv) **SMOS**: SMOS brightness temperatures assimilation only, with background error static during the whole assimilation cycle;

(v) **SMOS+Bprop**: SMOS brightness temperatures assimilation only, but permitting the propagation of the background error according to the SEKF equations. In this experiment, the model error was set to $0.01 m^3 m^{-3}$ at the start of the window for each model layer;

(vi) **SMOS+PI**: In this case the soil moisture analyses are substituted by the observed SMOS brightness temperatures projected in to control space. This approach gives maximum weight to the observations. However, in this experiment the SMOS observations are still subjected to the different quality controls applied in the SEKF, so at each time the observation is rejected the analysed soil moisture value is equal to its background;

(vii) **SMOS+2R**: SMOS brightness temperatures assimilation only, but doubling the error assigned to each observation, and therefore decreasing the influence of in the observations;

(viii) **SMOS+Btext**: SMOS brightness temperatures assimilation only, but the background error is a function of the water holding capacity (WHC), defined as the difference between the soil capacity and the wilting point. Given that the land model used in this study uses a global map of soil texture types, each of them with its own saturation and wilting point, the error in this experiment is a function of the soil texture type, and it will be larger for those soils with larger holding capacity, as organic type. An error of 10% of the WHC was assumed which, for a medium soil texture type, is equivalent to 20 mm of error integrated over the first metre of soil.

(ix) **SMOS+3DB**: SMOS brightness temperatures assimilation only, but assuming a 3D background model error. In this case, it is assumed that the short term variability and precipitation errors affect mainly the top layer, whereas the root-zone is less affected. An error of 20% of the WHC is set for the top layer, whereas this error is decreased to half for the second soil layer (7-28 cm), and only 5% for the third layer (28-100 cm).

The performance of these experiments, in terms of soil moisture analyses and atmospheric impact, was evaluated by combining them in three different groups, with the aim to study several aspects of the type of assimilated data and the observations or model uncertainties used in the SEKF:

1. Group I: **OL**, **SLV**, **SMOS** and **SLV+SMOS**: This first group of experiments was created to study the different type of observations assimilated in the SEKF and its influence on hydrological and atmospheric aspects. In this group, the **OL** experiment was used as the control experiment, and the atmospheric impact of all the other experiments were compared against this control.

2. Group II: **SMOS+PI**, **SMOS**, **SMOS+2R**: This second group of experiments is intended to investigate the effect of giving different weights to SMOS brightness temperatures when only this type of observation is assimilated.

3. Group III: **SMOS**, **SMOS+Bprop**, **SMOS+Btext**, **SMOS+3DB**: In this group the influence of different definitions of the background error covariance matrix in the analyses of soil moisture is investigated. Experiment **SMOS** was used as control and the atmospheric impact of the other experiments in this group was evaluated against this control.

Table 1 makes a summary of all the experiments and their main characteristics.

name	analysis	SLV	SMOS	σ_o^{SLV}	σ_o^{SMOS}	σ_b
OL	no	no	no	-	-	-
SLV	yes	yes	no	[2K,10%]	-	0.01
SMOS+SLV	yes	yes	yes	[2K,10%]	RA	0.01
SMOS	yes	no	yes	-	RA	0.01
SMOS-Bprop	yes	no	yes	-	RA	0.01
SMOS+PI	yes	no	yes	-	δ	0.01
SMOS+2R	yes	no	yes	-	2 x RA	0.01
SMOS-Btext	yes	no	yes	-	RA	$f(text)$
SMOS-3DB	yes	no	yes	-	RA	$f(text, depth)$

Table 1: Main characteristics of the experiments of this section. Each column represents the following: (1) experiment name, (2) is soil moisture analysed?, (3) are screen level variables (SLV) assimilated?, (4) are SMOS brightness temperatures assimilated?, (5) assumed observed error covariance for 2 m temperature and 2 m relative humidity [$\sigma^{T2m}, \sigma^{RH2m}$], (6) assumed SMOS brightness temperature observation error covariance (RA is the radiometric accuracy, δ is an infinitesimal number), (7) assumed background error covariance (in $m^3 m^{-3}$). 'f' represents a dependency, 'text' is soil texture, and 'depth' is the soil depth.

2.3 Validation and verification strategy

The validation of each of these experiments' soil moisture analyses was conducted by comparison against in-situ data from the U.S. Climate Reference Network (USCRN) and the Soil Climate Analysis Network (SCAN) in the US, following the same approach as in (Albergel et al. 2012); For the SCAN network, a total of 177 stations were used in this study. This network (http://www.wcc.nrcs.usda.gov/scan/) spans over all US, and provides comprehensive information of soil moisture and climate, designed to support natural resource assessments and conservation activities with a focus on agricultural areas in the United States. Long data records of soil temperature, soil moisture at several depths, soil water level, air temperature, relative humidity, solar radiation, wind, precipitation, and barometric pressure, among others, are available for this network. The vegetation cover at those sites consists of either natural fallow or short grass. Concerning soil moisture, data are collected by a dielectric constant measuring device, and measurements are typically made at 5, 10, 20, 50, and 100cm. The second network used to validate soil moisture analyses is the USCRN National from the Oceanic and Atmospheric Administration's National Climatic Data Center (USCRN NOAA's NCDC), consisting of 114 stations developed, deployed, managed, and maintained by NOAA. This network was built with the purpose of detecting the national signal of climate change. Soil moisture probes were installed at five standards depths; 5, 10, 20, 50 and 100 cm.

In this study both the top model layer and the root-zone layer analyses were validated. For the top layer the average of the 00, 06, 12 and 18 UTC daily analyses, representative of the first 7cm of soil, were compared to the daily average of the hourly in-situ observations located at a depth of 5 cm. For the root zone, the observations up to 1 m depth were used to build a weighted average proxy of root zone soil moisture. The measurements of all these probes were averaged daily and compared to the average of the daily 00, 06, 12 and 18 UTC analysis of the top three model layers, which are representative of the first metre of soil. The mean bias (MB), the root mean squared difference (RSMD) and correlation coefficient (R) of the analyses and in-situ data were computed for each station and averaged over the length of the experiment. Only significant correlation values were retained according to the p-value test, with a 5% confidence interval. Finally, for both networks, the mean statistics averaged over all the individual stations were computed.

The impact of these experiments in the near surface atmosphere was conducted by comparing the 2 m temperature and 2 m dew point temperature forecasts against observations from the SYNOP network. Fig. 1 presents the region within which SYNOP observations were retrieved and used for validation purposes. The impact of these experiments at short range forecasts and in the daily cycle were evaluated by using four synoptic forecast times: 12, 24, 36 and 48 h, respectively. A total of 30 forecasts were averaged for each synoptic time, based on forecasts started at 00UTC. Finally, the impact of an experiment in air temperature, air humidity, wind speed and geopotential height, compared to its control, was evaluated for several pressure levels: 1000 hPa (very close to the surface), 850 hPa (in the boundary layer), 500 hPa (in the troposphere) and 200 hPa (in the upper troposphere). The difference in root mean squared (RMS) forecast error between the experiment and its control, normalized by the control RMS, was computed at each time and averaged over 30 forecasts. The forecast error is defined in this study as the difference between the forecast and the operational analyses. The operational analysis was taken as reference as the observing system used in these experiments for the upper-air atmosphere is reduced, resulting in poorer analyses. In this case, the significance of the scores against their own analysis is less significant than using the operational analysis, which is of higher quality. Finally, the anomaly correlation of each group's experiment was evaluated up to 10 days of forecasts.

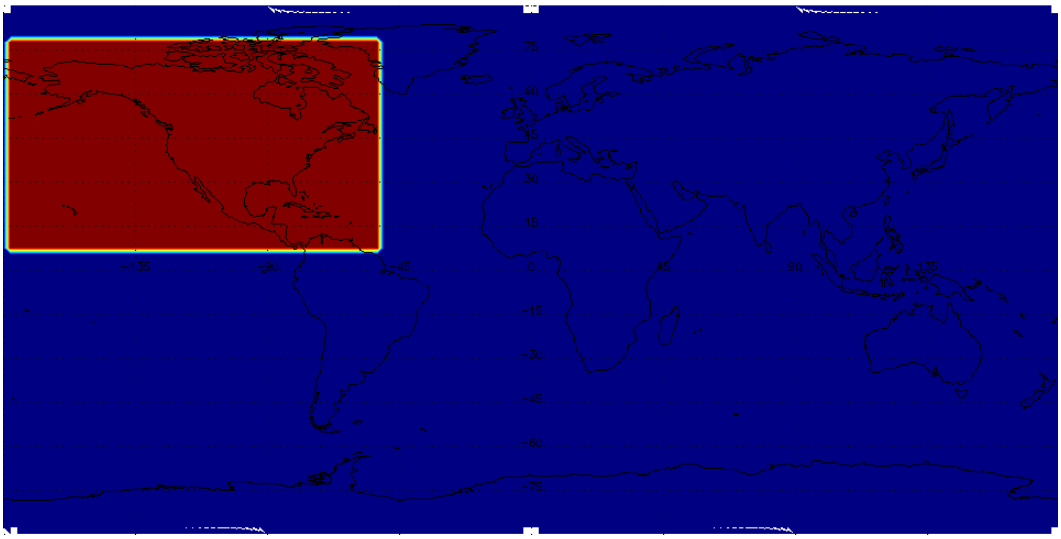

Figure 1: The red area shows the region that was used to study the influence of the experiments studied in this report in the forecast skill.

3 Results

3.1 Soil moisture validation

Tables 2, 3 and 4 show the validation of soil moisture analyses of experiments in group I, II and III, against all available observations from the USCRN and SCAN networks, respectively. These tables are split between the first model layer to which remote sensing observations are sensitive, and the first metre of soil where the plant roots extract water from the soil. In Table 2, the type of observing system experiments are investigated. For the USCRN network, 60 stations obtained correlation coefficients with significant values for the four experiments, whereas it was 86 for the SCAN network. The free soil moisture run configuration, **OL**, and the experiment assimilating screen temperature and humidity observations, **SLV**, obtained the largest bias and RMSD when compared to the averaged observations in the USCRN and SCAN networks. This occurred for both, the top layer and the root-zone. While this result was expected for the free run, as the model soil moisture is not constrained by any observation, one may expect better soil moisture with the screen-level constraint. However, we did not evidence any improvement compared to the free run. This result is in very good agreement with the study of (Drusch and Viterbo 2007), where the soil moisture analyses of an Optimal Interpolation scheme using screen variables were not superior to those forecasted by an open loop. The case presented here differs mainly in the use of an advanced assimilation scheme, the SEKF (Drusch et al. 2009), yet the results in terms of soil moisture are very similar to the open loop. Apart from the fact that screen-level data do not provide a direct observation of soil moisture, the combination of several other reasons can support these neutral results; firstly because the approach used in the SEKF is very conservative, giving very little weight to screen observations and therefore producing very small increments. Secondly because of the short period used in these experiments, which is not enough to observe the impact at longer time scales of the small screen data increments. And finally, even if screen data have been spatialised in a previous step, there is a small number of SYNOP observations influencing the analyses close to the stations of these networks. Locally for some stations, some differences are observed (not shown). However, introducing SMOS observations in the observation vector, either alone or in combination with screen variables, has a positive effect compared to the independent in-situ soil moisture observations, by reducing up to 43% the bias of the free run in average over the SCAN

network, and also having a positive impact in the RMSD. On the other hand, assimilating SMOS observations only, degrades the correlation coefficient. Fig. 2 shows the time series of soil moisture analyses for the four experiments, compared to the in situ observations, for a location where the soil is very dry and soil moisture has low variability during the studied period. It is observed that soil moisture in the **SMOS** experiment has larger variability compared to the other three, which for this type of dry soil penalises the correlation coefficient. The large variability of the analyses in **SMOS** experiment is not a good sign and it might points towards too small observation error assigned to the observations. The statistics obtained for the first metre of soil are in line with those of the first layer. These results are encouraging, as they show the potential benefit introduced by SMOS data not only for the first layer, but also for the layer more relevant for NWP impact due to its strong influence on evapotranspiration fluxes.

		USCRN				SCAN			
	expt	**MB**	**RMSD**	**R**	**N**	**MB**	**RMSD**	**R**	**N**
0-7 cm	**OL**	-0.115	0.130	0.75	60	-0.062	0.104	0.74	86
	SLV	-0.115	0.130	0.75	60	-0.061	0.104	0.74	86
	SMOS+SLV	-0.097	0.121	**0.76**	60	-0.048	**0.101**	**0.75**	86
	SMOS	**-0.089**	**0.115**	0.67	60	**-0.035**	**0.101**	0.68	86
1-100 cm	**OL**	-0.089	0.096	**0.74**	37	-0.032	**0.096**	**0.74**	56
	SLV	-0.089	0.096	0.72	37	-0.031	**0.096**	0.70	56
	SMOS+SLV	-0.087	0.095	0.72	37	-0.030	**0.096**	0.72	56
	SMOS	**-0.080**	**0.089**	0.61	37	**-0.024**	0.099	0.61	56

*Table 2: Mean Bias (MB), Root Mean Square Difference (RMSD) and correlation coefficient (R) values between the **expt** type soil moisture analyses and in-situ observations for USCRN and SCAN networks. Only significant correlation values are used using the p-value test with a 5% confidence interval. **N** is the number of stations with significant correlation values for all the experiments compared in this table. For the first metre of soil, in-situ observations averaged at depth of 5, 10, 20, 50 and 100 cm were averaged and compared to the average of soil moisture analyses.*

Table 3 shows the validation results for group II of experiments. Here the different weight given to the observations when only SMOS T_B are assimilated is investigated. It is observed that the **SMOS** experiment, which assigns the radiometric accuracy to each observation as the error characterizing the SMOS observed T_B, obtains the best results in terms of lower bias and RMSD for the top layer. The improvement is better for the SCAN network. However, as it occured in Fig. 2, the larger variability of the observations in the **SMOS** experiment penalises the correlation coefficient. By doubling the error of SMOS observations the gain is smaller, and so are the increments. This is beneficial for the correlation coefficient for just a month of analyses, but it is necessary to investigate longer assimilation periods, including at least a whole season, to understand the effect of the lower increments in terms of RMSD and correlation coefficient. Not surprisingly, using the direct insertion of SMOS observations into model space as soil moisture analyses obtains the worst results in terms of bias and RMSD, at least for the SCAN network. Although in **SMOS+PI** unrealistically large influence is given to the observations, which should be reflected into larger increments, one should bear in mind that the SEKF quality checks still apply in this case (first-guess check, jacobian check and excessive soil moisture correction), preventing too large spurious adjustment of soil moisture. This explains the relatively good correlation values. The RMSD and mean bias for the root-zone are still better for the **SMOS** experiment, but the differences are much smaller compared to the other experiments. In this case, the Jacobians propagate the information into the deeper layer and they are equivalent for the three experiments, so the values are much closer.

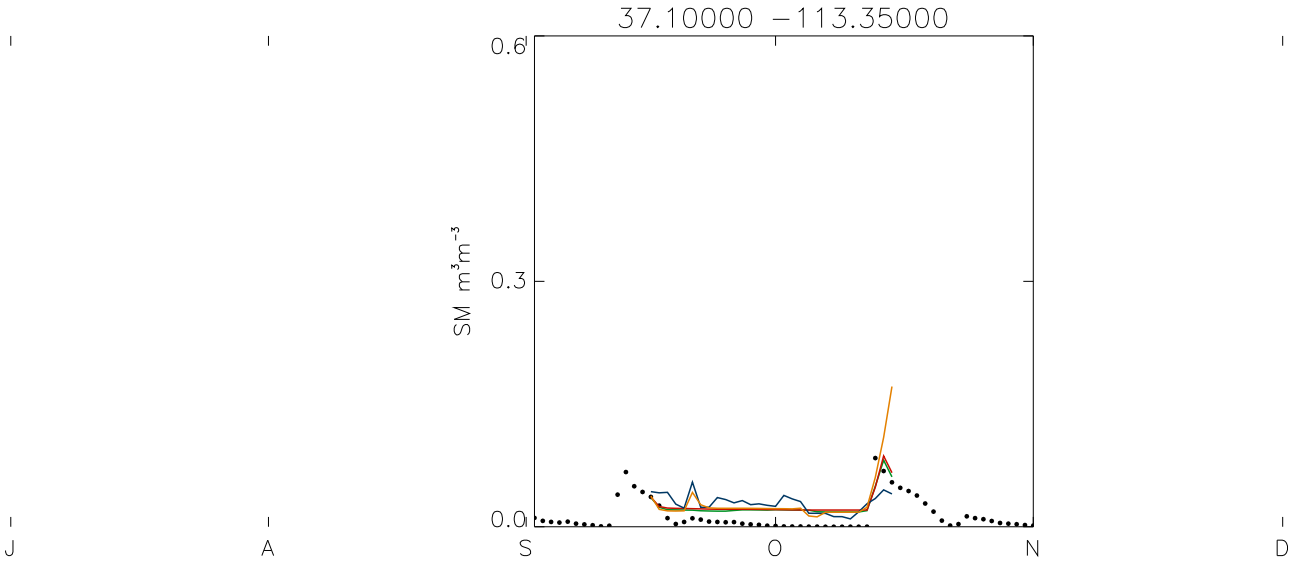

*Figure 2: Soil moisture time series for the analyses of **OL** (red curve) **SLV** (green curve) **SMOS** (dark blue curve) and **SLV+SMOS** (orange curve) experiments. The daily averaged observations for this station of the SCAN network in US are displayed in black dots.*

		USCRN				SCAN			
	expt	**MB**	**RMSD**	**R**	**N**	**MB**	**RMSD**	**R**	**N**
0-7 cm	**SMOS+PI**	-0.099	0.116	0.71	58	-0.051	0.106	0.68	83
	SMOS	**-0.086**	**0.113**	0.69	58	**-0.032**	**0.101**	0.69	83
	SMOS+2R	-0.096	0.117	**0.74**	58	-0.044	0.104	**0.72**	83
1-100 cm	**SMOS+PI**	-0.082	0.092	**0.70**	38	-0.029	0.095	**0.67**	62
	SMOS	**-0.081**	**0.091**	0.63	38	**-0.025**	0.095	0.58	62
	SMOS+2R	**-0.081**	**0.091**	**0.70**	38	-0.027	0.095	0.65	62

*Table 3: As Table 2 but the experiment types in this table assimilate only SMOS brightness temperatures, giving different weight to the observations: **SMOS+PI** (soil moisture analysis are substituted directly by projecting the SMOS brightness temperature observation in the state space), **SMOS** (with the R matrix as defined previously) and **SMOS+2R** (doubling the error of the SMOS observations in the SEKF.*

Table 4 presents the statistics for the group III of experiments, investigating in this case the role of different definitions of the background error covariance matrix in the analysis of soil moisture. Soil physiographic parameters will either enhance or reduce the variability of soil moisture. They will depend among others of soil texture, being the latter a key parameter in soil moisture prediction. Introducing soil texture information in the specification of the background error matrix has a positive effect in soil moisture analysis of the top layer, as shown in Table 4. Either in **SMOS-Btext** or **SMOS-3DB** soil texture information is accounted for in the uncertainty of the background error through the water holding capacity. This has a positive effect in terms of bias and RMSD of the top layer, being the results very similar for both types of experiments. On the contrary, the correlation coefficient is worse compared to **SMOS** and **SMOS-Bprop**, which do not add information of

soil texture. Both, in **SMOS-Btext** or **SMOS-3DB**, the background error is increased, and that increases also the gain and the increments, producing increments with stronger variability. The propagation of the **B** matrix is affected by a constant model error, in this particular case it was fixed to $0.01 m^3 m^{-3}$). In this study, the assimilation window has a length of 12 h. However, this does not have a significant effect in the statistics compared to **SMOS**, likely due to the fact that the **B** matrix is reinitialized at the next cycle. For the root zone, the differences are smaller, but the definition of a more realistic vertical structure of errors (decreasing with depth) showed to be positive on the correlation coefficient with in-situ data, at least over the USCRN network, whereas more neutral results were obtained for SCAN.

		USCRN				SCAN			
	expt	**MB**	**RMSD**	**R**	**N**	**MB**	**RMSD**	**R**	**N**
0-7 cm	**SMOS**	-0.085	0.109	**0.70**	64	-0.022	0.095	**0.70**	77
	SMOS-Bprop	-0.088	0.111	0.69	64	-0.025	0.095	**0.70**	77
	SMOS-Btext	-0.074	0.104	0.67	64	**-0.015**	**0.094**	0.66	77
	SMOS-3DB	**-0.071**	**0.102**	0.65	64	-0.016	**0.094**	0.64	77
1-100 cm	**SMOS**	-0.077	0.093	0.63	30	-0.013	0.090	0.64	48
	SMOS-Bprop	**-0.076**	**0.091**	0.65	30	**-0.012**	0.090	**0.65**	48
	SMOS-Btext	-0.077	0.092	0.66	30	**-0.012**	0.090	0.64	48
	SMOS-3DB	**-0.076**	0.092	**0.71**	30	**-0.012**	**0.089**	**0.65**	48

*Table 4: As Table 2 but in this table the performance of different definitions of the **B** matrix is studied: In **SMOS** the **B** matrix is fixed, whereas in **SMOS-Bprop** it is propagated in time until the next cycle. **SMOS-Btext** and **SMOS-3DB** introduce the information of soil texture in the background error.*

3.2 Two metre temperature and dew point temperature validation

Due to the coupled nature of the IFS, it is expected that the state of the soil have an impact on atmospheric variables having a strong link with soil moisture. In this section, the performance of 2 m temperature and 2 m dew point temperature (from which relative humidity is derived) forecasts against SYNOP observations was investigated, as described in section 2.3. Fig 3 and Fig. 4 show the results for group I, in terms of forecast bias and RMS forecast error as a function of four synoptic times. For 2 m temperature, biases follow a clear diurnal cycle, being stronger at 12 UTC (which is early in the morning in local time in US) due to more stable conditions of the boundary layer, whereas biases are smaller in the evening as the gradients of temperature are smaller in a well mixed boundary layer. The free run introduces the largest forecast bias at all lead times except early in the morning, when the **SMOS** experiment obtains the largest biases. The opposite occurs in the evening. The RMS forecast error is larger early in the morning than in the evening, with the free run obtaining the largest error with the forecast lead time. The same is observed for the 2 m dew point temperature, with the errors getting substantially larger with the lead forecast time. For this variable, although small, the model is affected by a cold bias for all 4 synoptic times. The experiment assimilating only SLV obtains the lowest bias as indeed the assimilation system was designed to minimize errors in screen variables. Figs 5 and Fig. 6 show the equivalent results obtained for group II of experiments. The level of biases are similar of those presented in Figs. 3 and 4. In terms of RMS forecast error of 2 metre temperature, the results are very similar, slightly lower errors for the **SMOS** experiment which are in line with those presented in Table 3. However, the diurnal cycle of biases makes them being larger early in the morning for the **SMOS** experiment, and the lowest during the evening. Larger differences are found in terms of 2 m dew point temperature, but the results are consistent with those

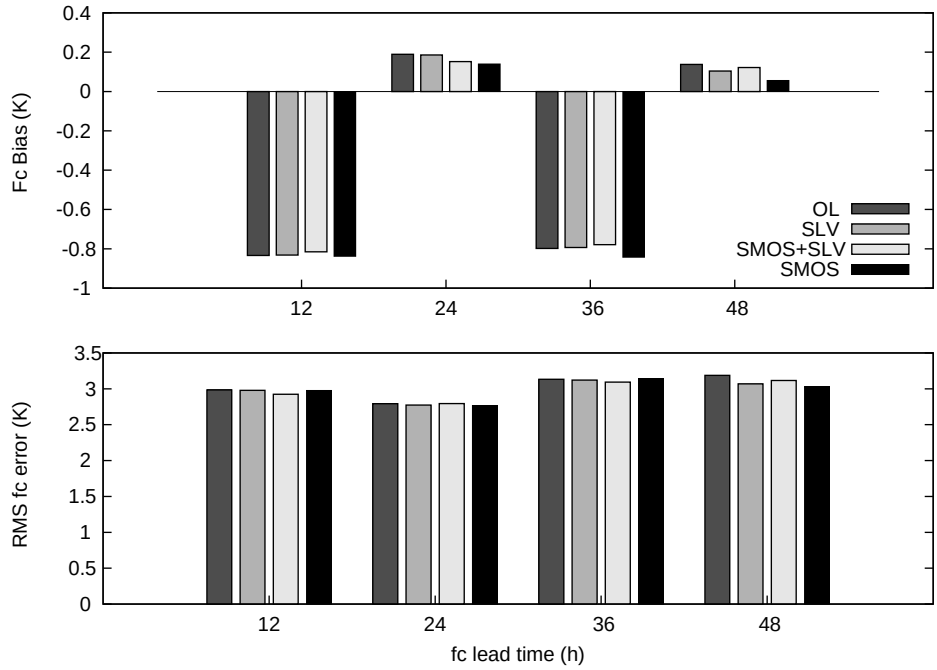

Figure 3: Forecast bias and RMS forecast error of 2 metre temperature compared to observations of the SYNOP network in North America, as a function of the forecast lead time for the four experiments of group I.

of 2 m temperature. After 36 h forecast, doubling the specified observation error of the SMOS observations decreases slightly the RMS forecast errors and biases compared to the other experiments. Figs 7 and Figs 8 show the equivalent results for group III. For 2 m temperature, the results are very similar, with **SMOS-3DB** obtaining the lowest forecast biases in the morning and the largest in the evening, but the differences are very small. In terms of 2 m dew point temperature, **SMOS-Bprop** has the largest biases, whereas they are very similar in RMS.

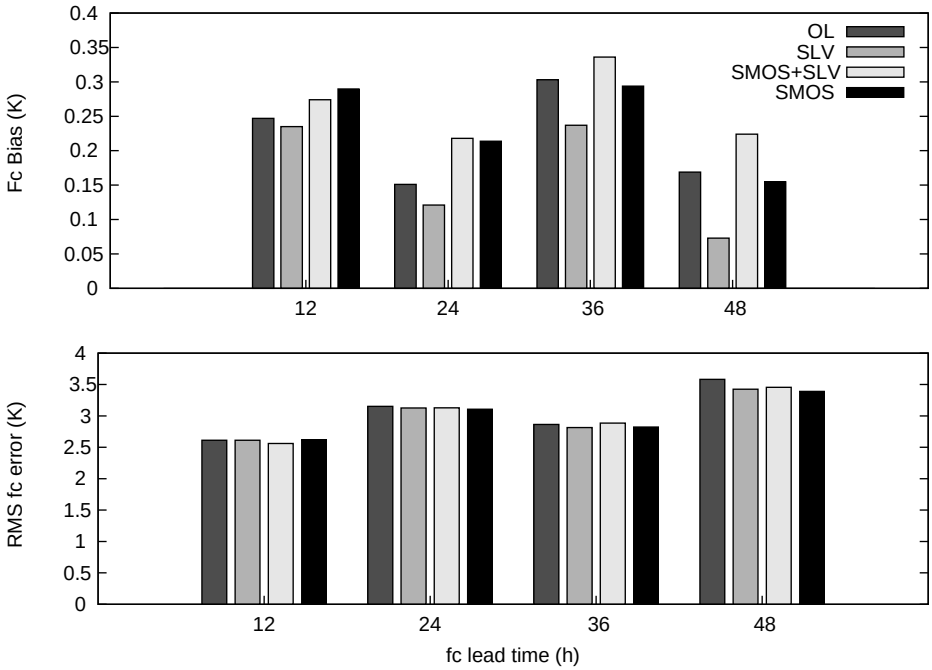

Figure 4: As fig. 3 but for 2 m dew point temperature.

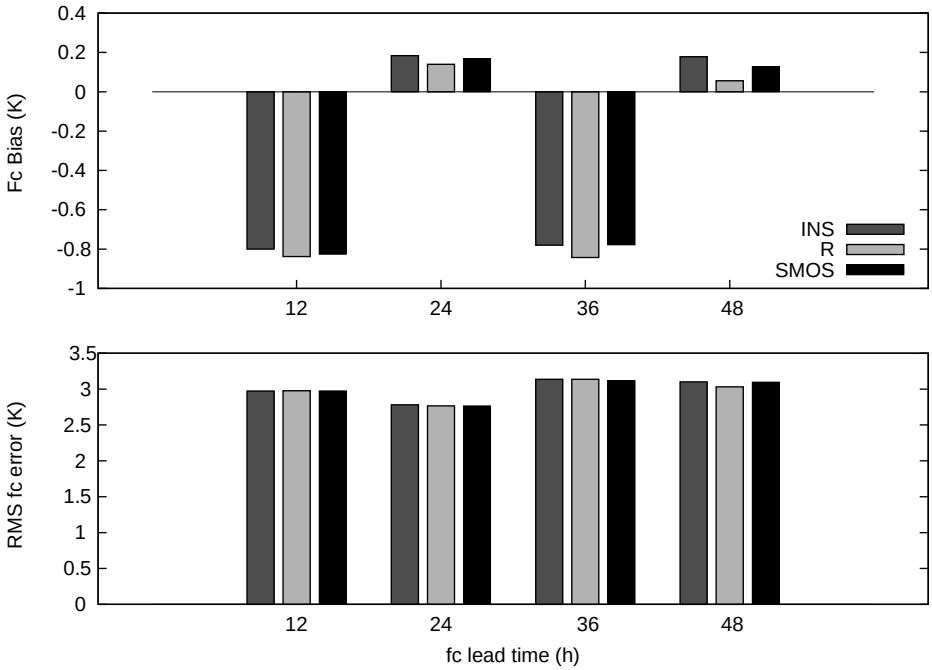

Figure 5: As Fig. 3 but for the experiments of group II.

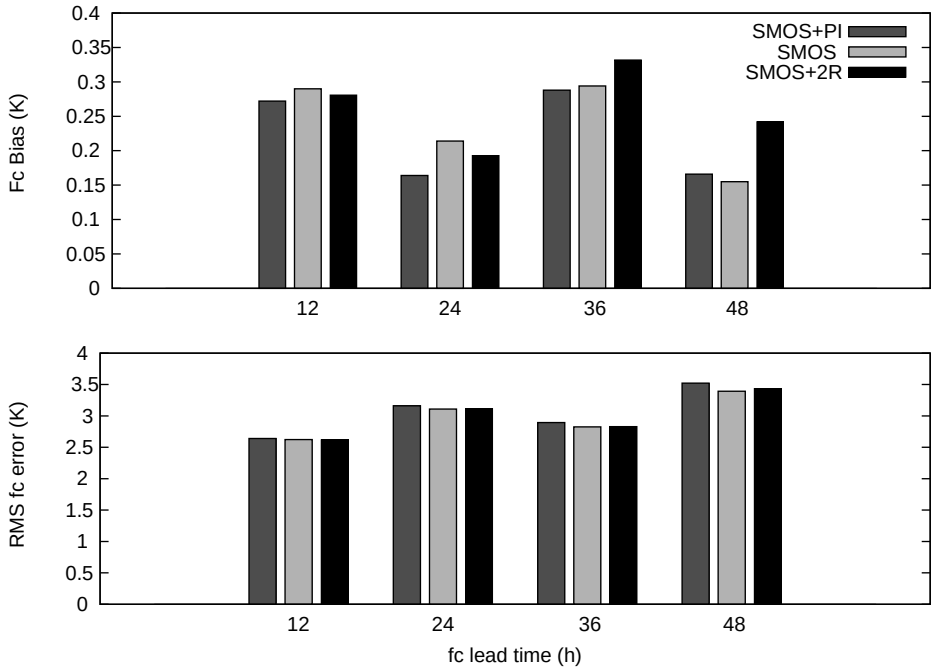

Figure 6: As Fig. 3 but for the experiments of group II and for 2 m dew point temperature.

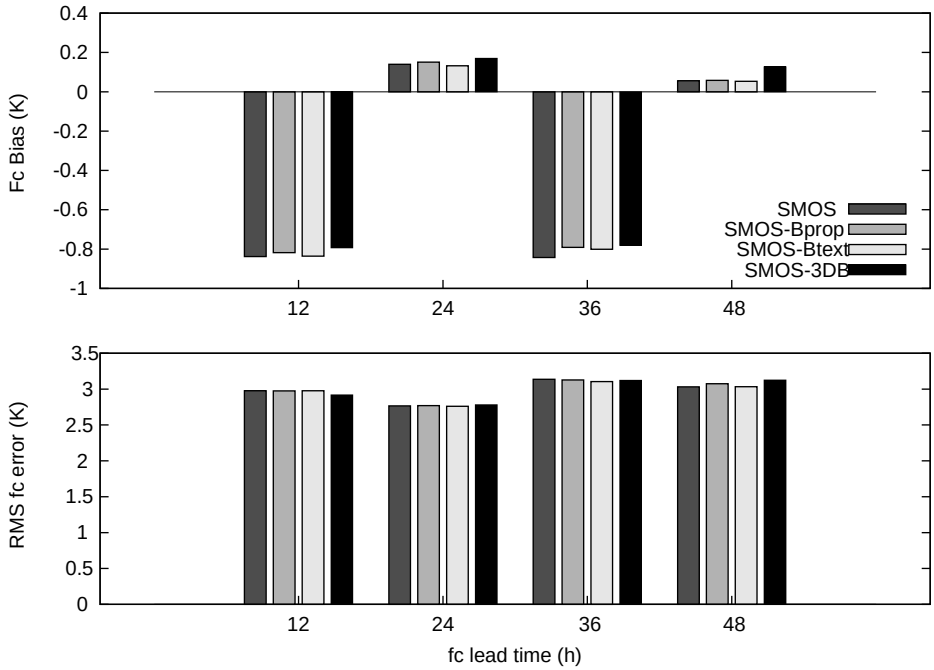

Figure 7: As Fig. 3 but for the experiments of group III.

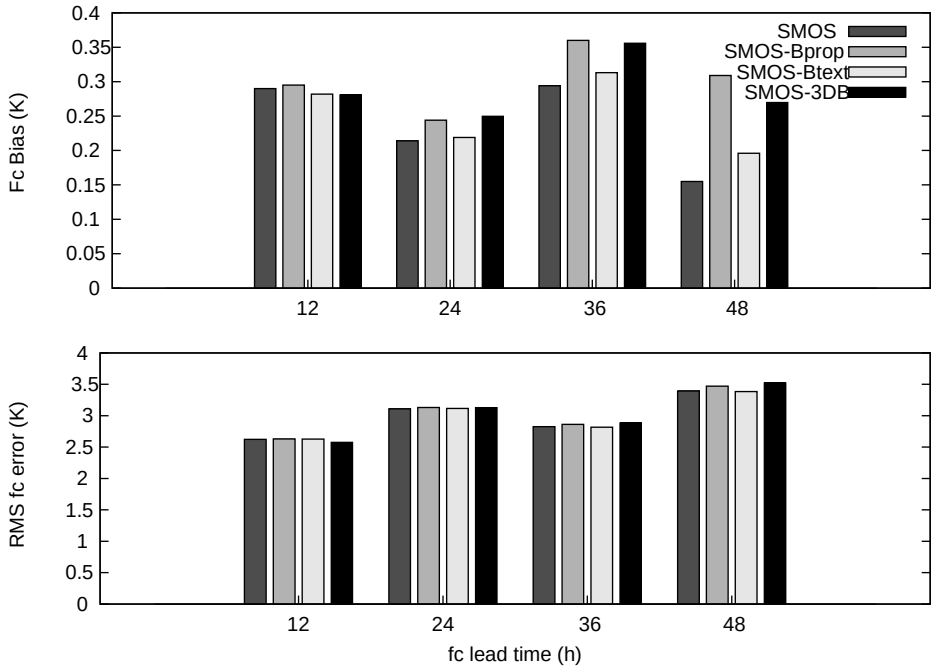

Figure 8: As Fig. 3 but for the experiments of group III and for 2 m dew point temperature.

3.3 Atmospheric impact

In this section the sensitivity of the atmospheric scores to the different error scenarios of this report is analysed. Given that SMOS observations were assimilated only over North America, the mask displayed in Fig. 1 (in addition to a land-sea mask) was applied in order to obtain statistics only for North America. In total, 30 forecasts from 15 September to 14 October 2012 were run up to 240 hours. As reference, the operational analyses was selected. Fig. 9 shows, for the group I of experiments, the root mean square forecast error normalized by the forecast error of the control, at four pressure levels (1000, 850, 500 and 200 hPa) and for air temperature and air humidity. The error bars show the 95% confidence intervals. Negative values indicate that the forecast error of the experiment compared to the control **OL** has decreased. It is observed that, in general, better scores are obtained for all pressure level and for the three experiments compared to the free run. This result reinforces the importance of analysing soil moisture. Scores are especially positive for air temperature and better closer to the surface, with improvements that can be close to 20% if only screen level variables are assimilated, and with significant values up to 7 days. The scores on air temperature and humidity are equally positive if SMOS data is assimilated (along with screen temperature and humidity or not), but they are not as positive as for the **SLV** experiment. In particular, after day 4, the improvement decreases quickly if only SMOS observations are assimilated. For air humidity scores can be significantly improved more than 10% if screen variables are assimilated and with significant values up to 8 days. In the appendix, the scores for the vector wind and geopotential height are shown in Fig. 18. Consistently with air temperature and air humidity, geopotential height and the wind vector are also improved by similar levels, from 10% to 20% and being better for the experiment using screen observations only.

The absolute value of the RMS forecast error is shown in Figs. 10 and 19 (in the appendix). It is observed how it grows with the forecast time, from as little as 0.8 K (5.5%) at 12 h air temperature (air humidity) forecast to more than 4 K (15%) at 10 days forecast close to the surface, whereas errors get larger higher in the atmosphere especially for air humidity which can be doubled at 200 hPa. The **SLV** experiment corresponding to the black curve obtains the lowest errors, followed by the **SLV+SMOS** (green curve), **SMOS** (red curve) and finally **OL**

(blue curve), which obtains the largest errors. By assimilating screen variables, the RMS forecast error of air temperature compared to **OL** decreases by 0.7 K at 5 day forecast and 1000 hPa, 1.5% for air humidity, 1 m/s for the wind vector and up to 150 m for geopotential height. In Fig. 11 the mean forecast error (verified against the operational analysis) is presented for air temperature and air humidity. The air in **SLV+SMOS** experiment gets colder in the boundary layer, although the cooling is limited to 0.3 K. For this atmospheric levels, the other experiments are more in agreement with the operational analyses. Close to the surface, the air is also more humid compared to the operational analyses, being the **OL** experiment that presenting a more humid forecast air. Compared to the free run, the assimilation experiments of group I improve the anomaly correlation, about 1 day at 60% if screen level data is assimilated, and half a day if only SMOS observations are assimilated, as observed in Fig. 12. Figs 19 and 20, in the appendix, present the results for the geopotential height too, which are in line with those of air temperature and humidity. The atmospheric impact of this first set of experiments shows the importance of constraining soil moisture by observations, either indirectly through screen variables or directly through remote sensing data. However, although these results are quite positive, in the interpretation of these results one should consider different aspects; firstly, the period of analysis only includes one months of forecasts. This makes the error bars in Figs 9 (and other similar plots) quite large, and frequently the scores are not significant. And secondly these results may be amplified by the fact of using a poor observational system to constrain the atmosphere. One consequence is the presence of a poor background value, which may produce strong atmospheric increments and spuriously intensify the atmospheric impact, in particular in the stratosphere.

The results obtained for the air temperature and air humidity normalized RMS forecast error of group of experiments II are presented in Figs. 13, and for the vector wind speed and geopotential height in the appendix (see Fig. 21). Contrarily to group I, the sensitivity in the skill of the forecast is much reduced, being most of the time neutral. For air temperature, a significant degradation up to 4% is observed for **SMOS+PI** compared to **SMOS**, and up to 2 days for air humidity close to the surface. Giving excessive weight to the observations produces spurious increments with negative effects in the atmospheric scores. The results are quite neutral, with a slight improvement in air humidity close to the surface, if the SMOS observation error is doubled. In terms of absolute RMS forecast error, similar values to the first group of experiments was observed (see Fig. 14), but in this case the differences between the three experiments of this group are very small. It is worth mentioning that either giving more or less weight to the SMOS observations, the mean forecast error of air temperature increased close to the surface compared to the operational analyses, whereas it was quite neutral for air humidity. As expected from the previous results, the anomaly correlation is slightly degraded for the pseudo-insertion experiment and for the first few forecast days, whereas is positive-neutral (although with a positive trend) if the error is doubled (see Fig. 15 for the normalized anomaly correlation.). The anomaly correlation scores for the geopotential height are presented in Fig. 22.

The atmospheric impact of the third group of experiments is shown in Figs. 16 and 23. Either for air temperature or air humidity, **SMOS-Btext** obtains the best scores compared to the **SMOS** experiment, being neutral to positive. Contrarily **SMOS-3DB** does not improve the scores of **SMOS**, being in this case neutral to negative. Consistenly, Fig. 17 shows that the anomaly correlation is the best for **SMOS-Btext** after day-4 close to the surface for air temperature, whereas **SMOS-3DB** obtains the worse anomaly correlation after day 2. For air humidity **SMOS** is slightly better than **SMOS-Btext** after day-4. The scores for the geopotential height are shown in Fig. 24 of the appendix.

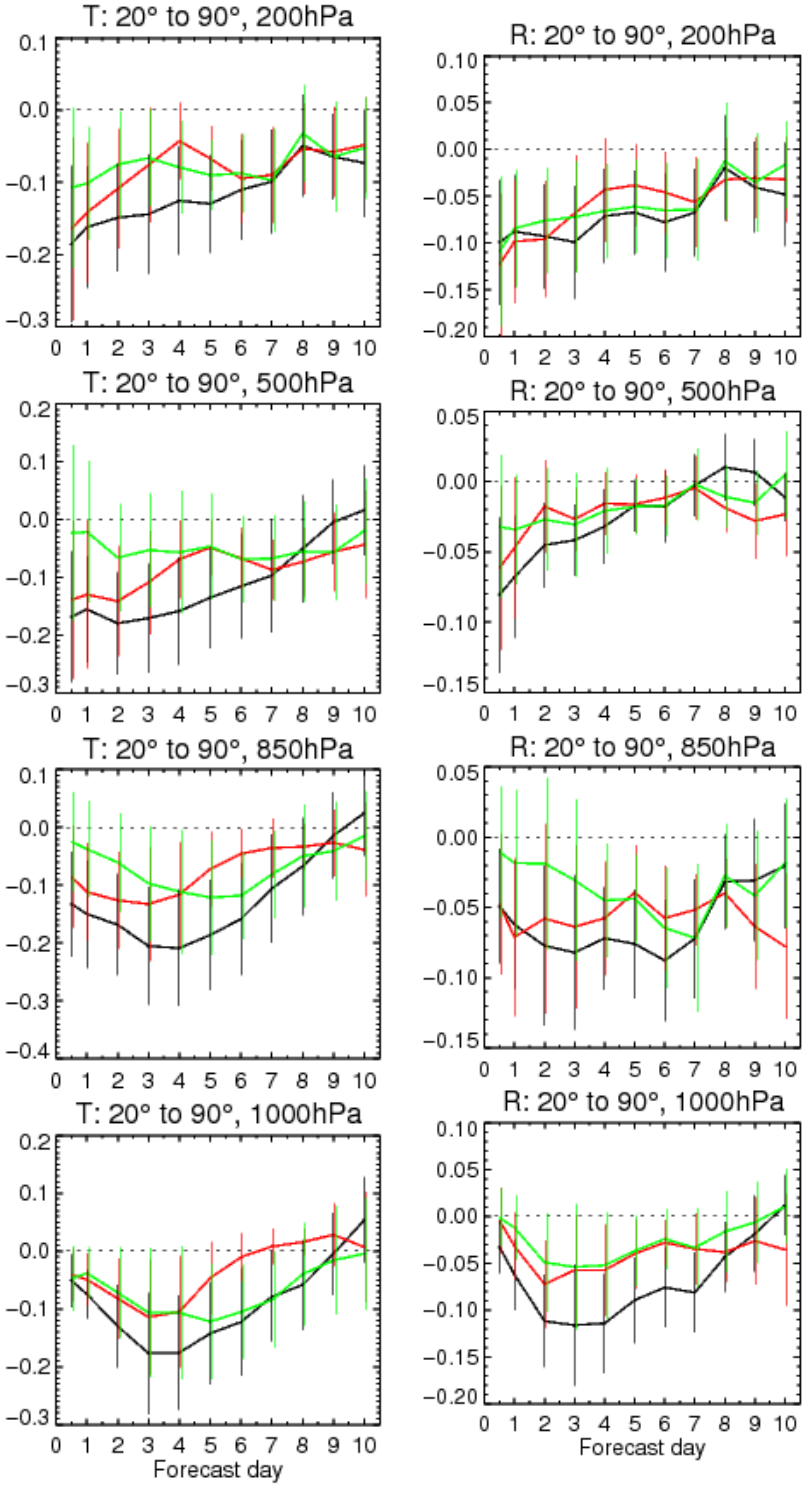

*Figure 9: Air temperature (left panel) and air humidity (right panel) normalized root mean square forecast error of **SLV** (black curve), **SMOS** (red curve) and **SLV+SMOS** (green curve) experiments compared to the control **OL** experiment, as a function of the forecast lead time. Scores are shown for four different pressure levels: 1000 (bottom), 850 (middle bottom), 500 (middle top) and 200 hPa (top). The operational analyses are used as reference. Error bars show 95% confidence intervals.*

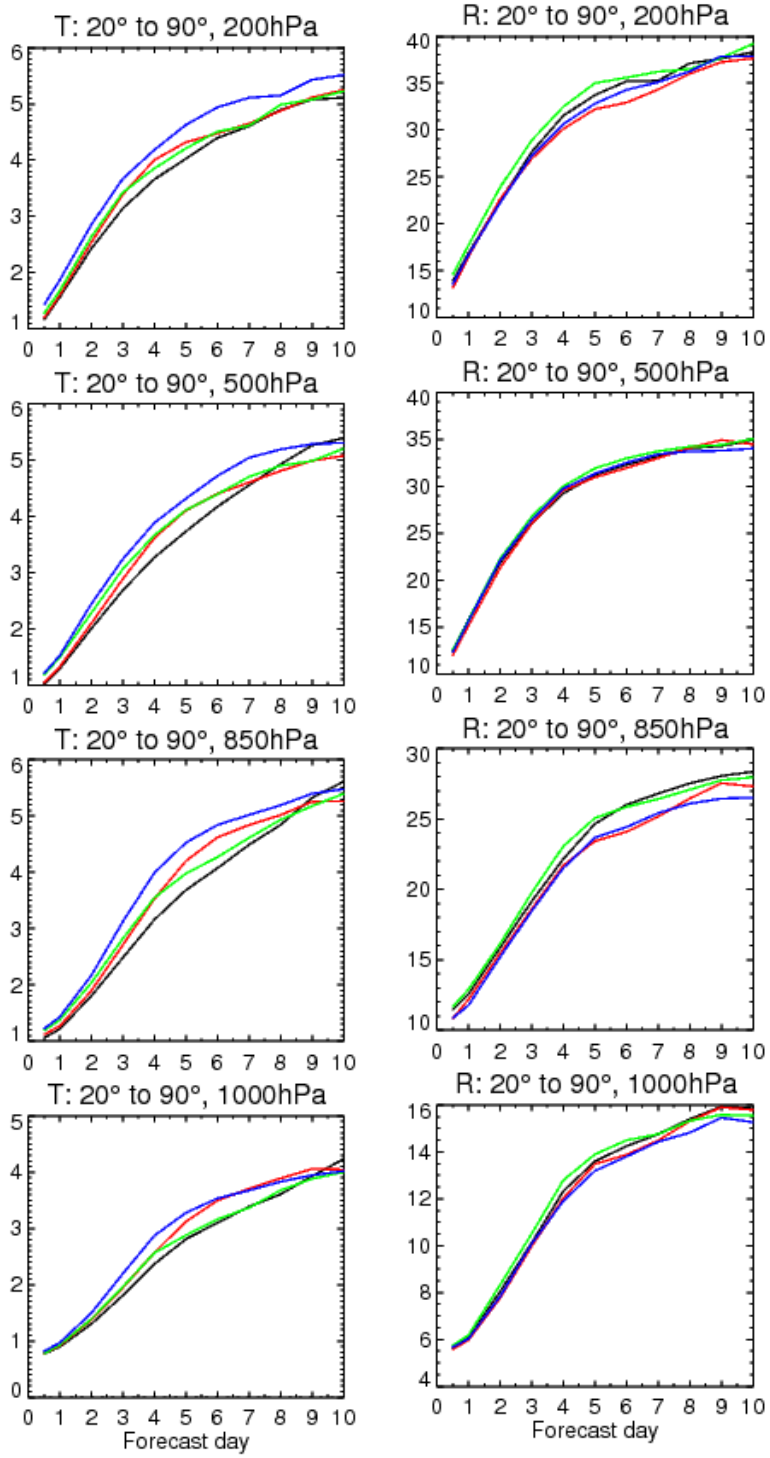

*Figure 10: Air temperature (left panel) and air humidity (right panel) root mean square forecast error of the **OL** (blue curve), **SLV** (black curve), **SLV+SMOS** (green curve) and **SMOS** (red curve) experiments, as a function of the forecast lead time. Scores are shown for four different pressure levels: 1000 (bottom), 850 (middle bottom), 500 (middle top) and 200 hPa (top). The operational analyses are used as reference.*

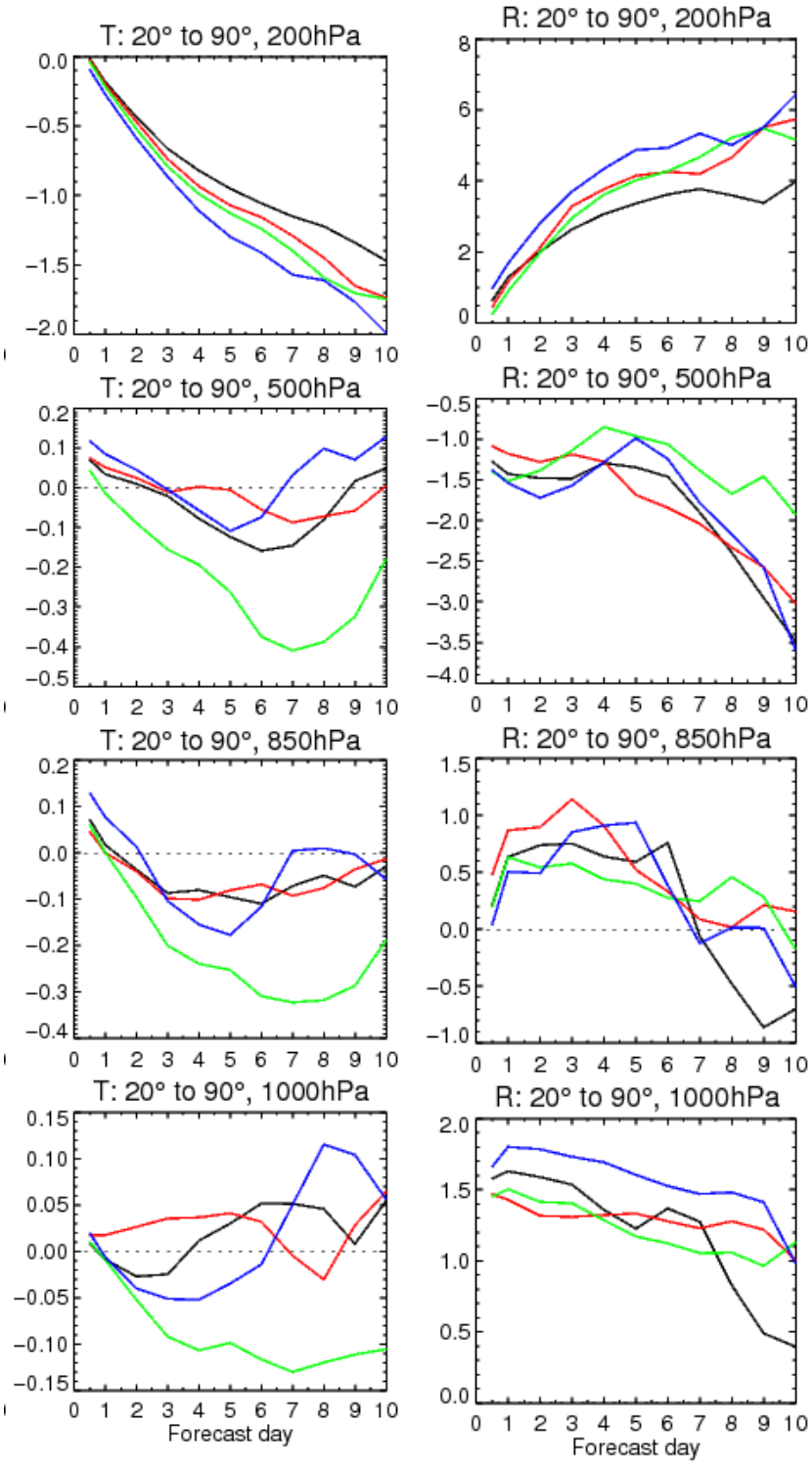

*Figure 11: Air temperature (left panel) and air humidity (right panel) mean error (verified against the operational analysis), averaged over North-America as a function of the forecast lead time, for **OL** (blue curve), **SLV** (black curve), **SLV+SMOS** (green curve) and **SMOS** (red curve) experiments. Scores are shown for four different pressure levels: 1000 (bottom), 850 (middle bottom), 500 (middle top) and 200 hPa (top).*

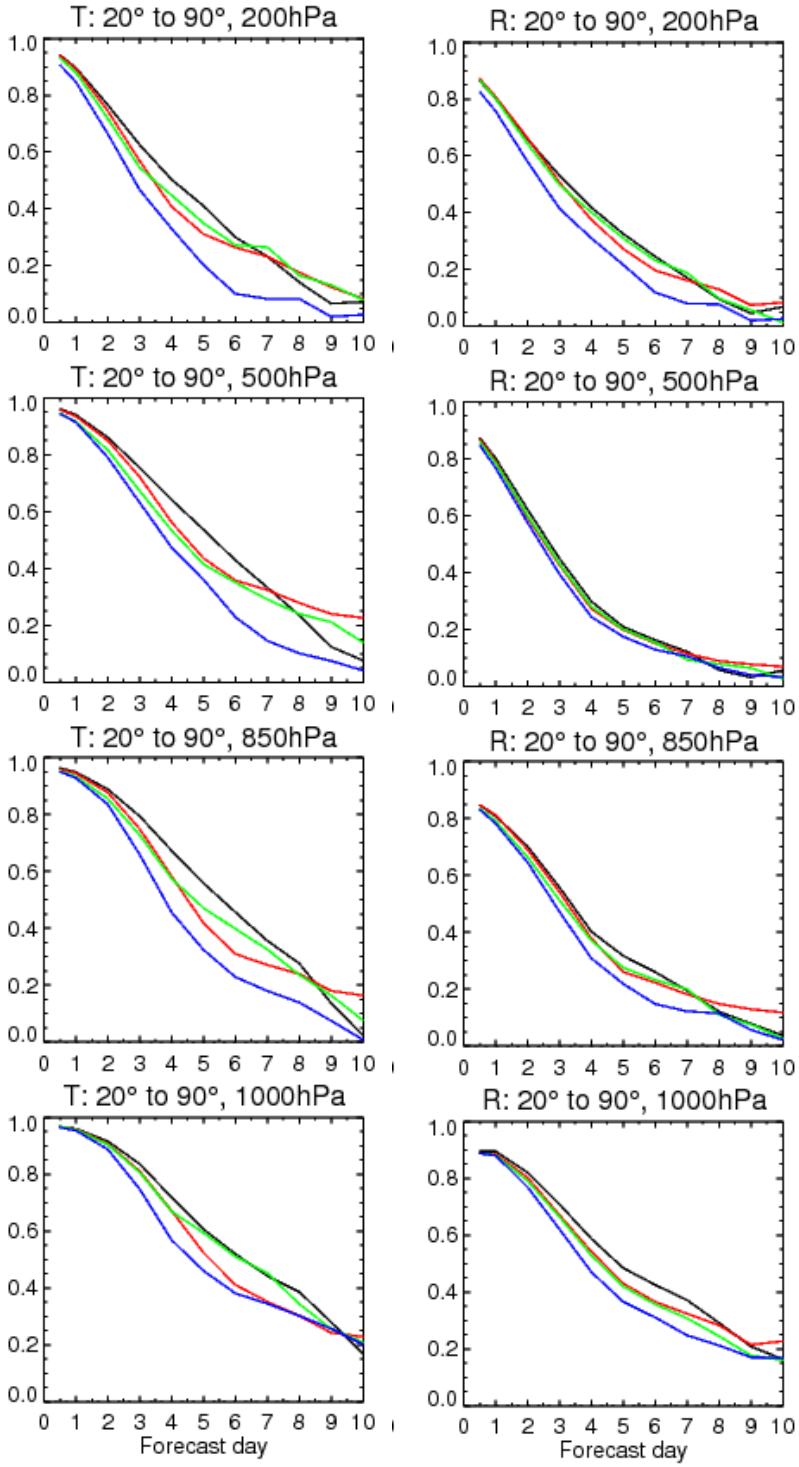

*Figure 12: Air temperature (left panel) and air humidity (right panel) anomaly correlation verified against the operational analyses as a function of the forecast lead time, for **OL** (blue curve), **SLV** (black curve), **SLV+SMOS** (green curve) and **SMOS** (red curve) experiments. Scores are shown for four different pressure levels: 1000 (bottom), 850 (middle bottom), 500 (middle top) and 200 hPa (top).*

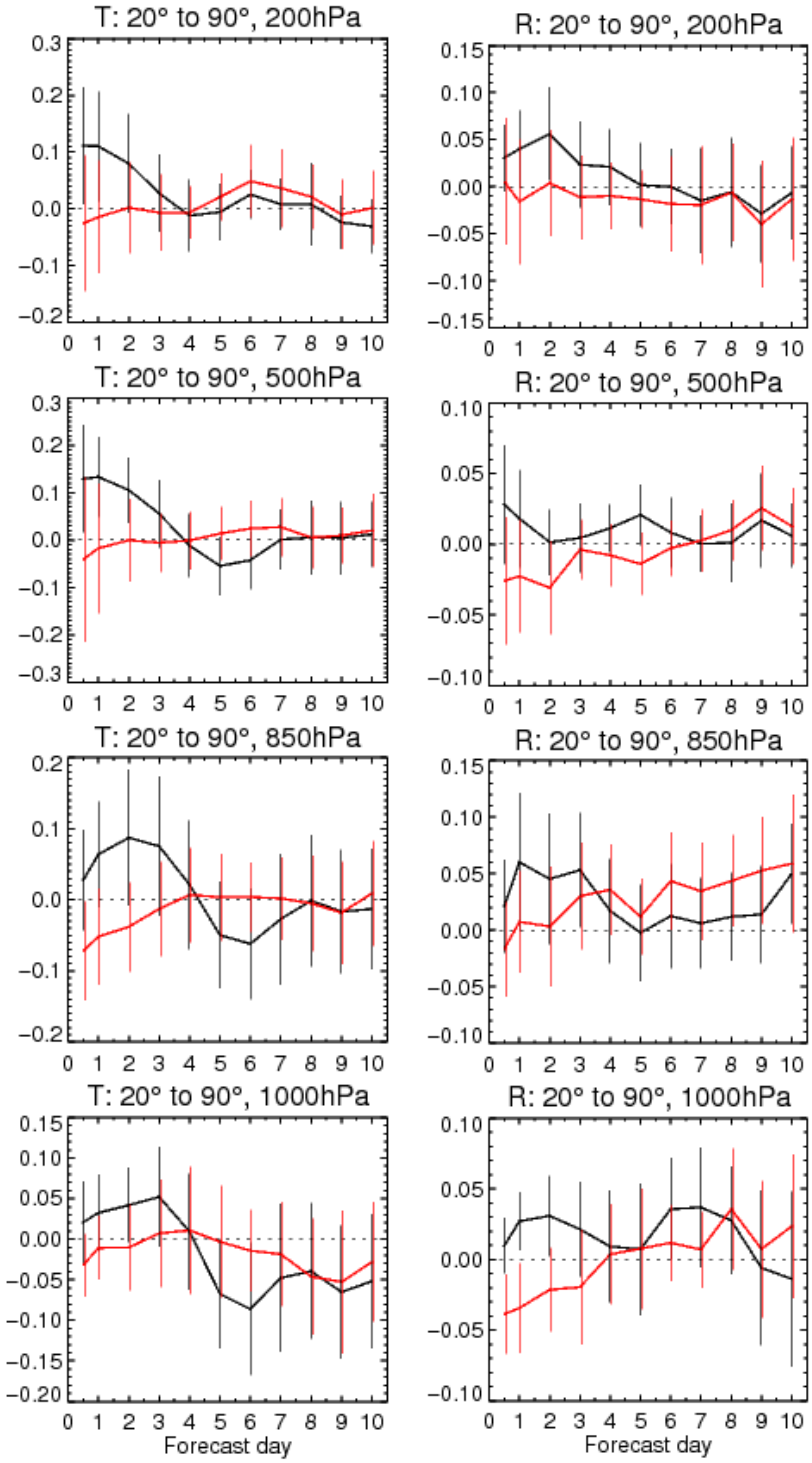

*Figure 13: Air temperature (left panel) and air humidity (right panel) normalized root mean square forecast error of **SMOS+PI** (black curve) and **SMOS+2R** (red curve) experiments compared to the control **SMOS** experiment, as a function of the forecast lead time. Scores are shown for four different pressure levels: 1000 (bottom), 850 (middle bottom), 500 (middle top) and 200 hPa (top). The operational analyses are used as reference. Error bars show 95% confidence intervals.*

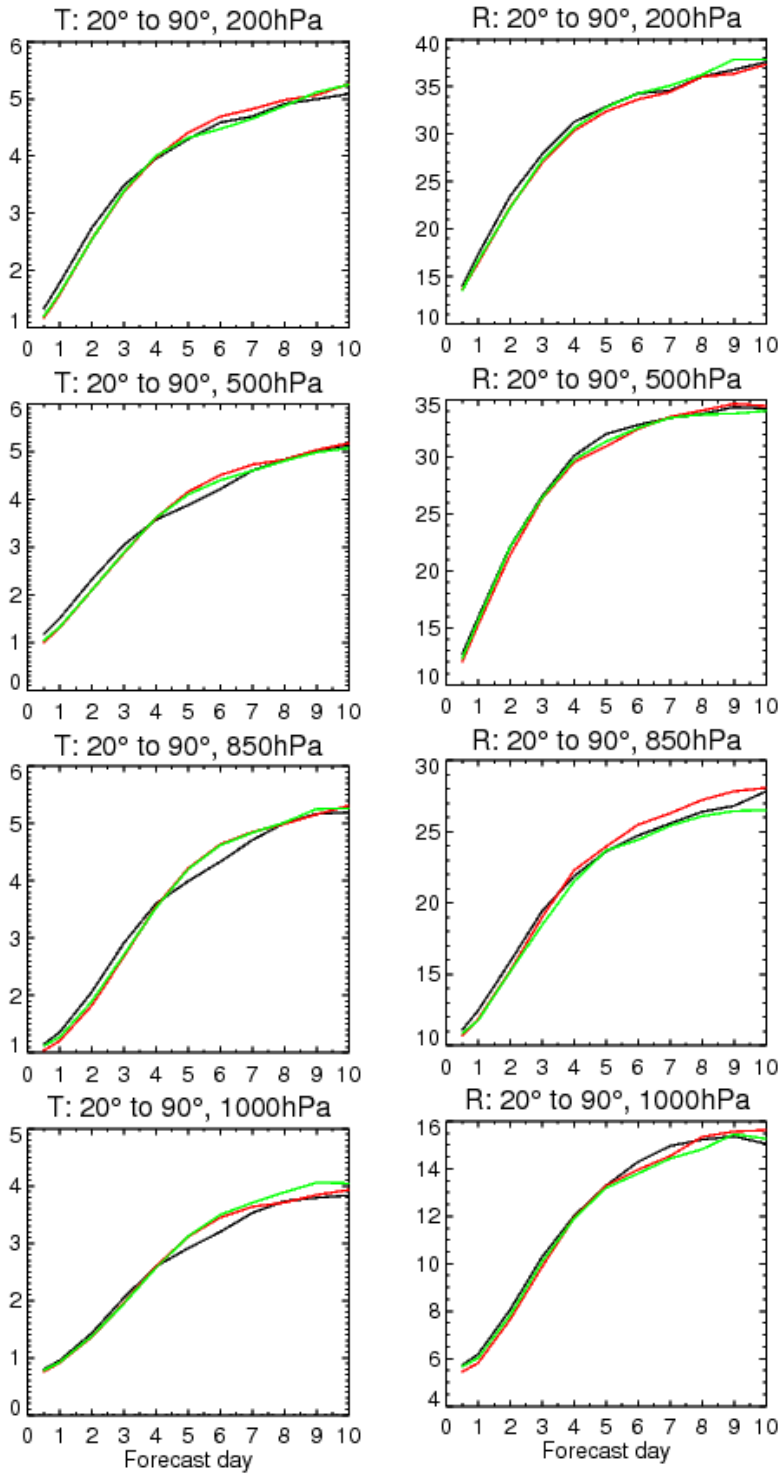

*Figure 14: Air temperature (left panel) and air humidity (right panel) root mean square forecast error of the **OL** (blue curve), **SLV** (black curve), **SLV+SMOS** (green curve) and **SMOS** (red curve) experiments, as a function of the forecast lead time. Scores are shown for four different pressure levels: 1000 (bottom), 850 (middle bottom), 500 (middle top) and 200 hPa (top). The operational analyses are used as reference.*

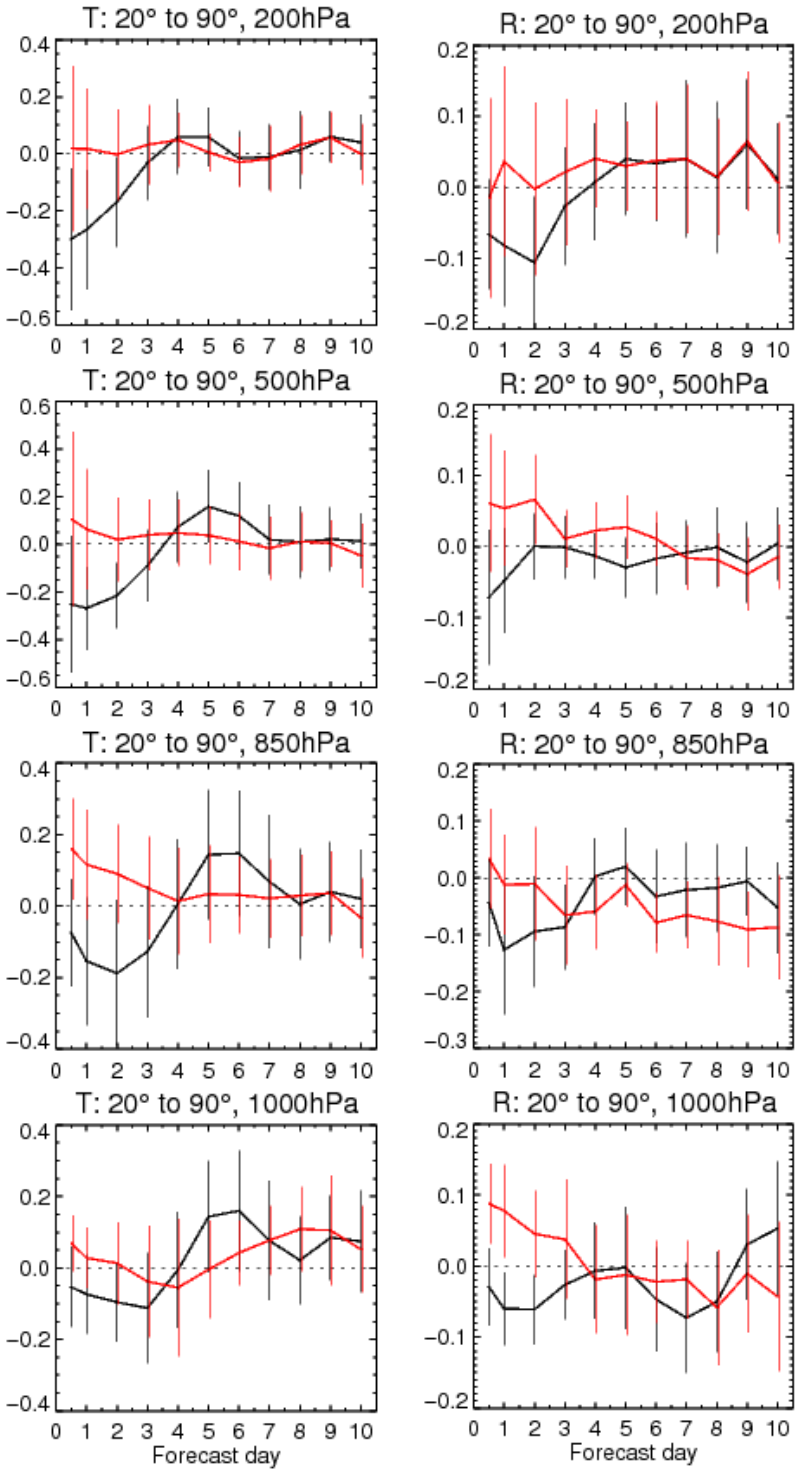

*Figure 15: Air temperature (left panel) and air humidity (right panel) normalized anomaly correlation of **SMOS+PI** (black curve) and **SMOS+2R** (red curve) experiments compared to the control SMOS experiment, as a function of the forecast lead time. Scores are shown for four different pressure levels: 1000 (bottom), 850 (middle bottom), 500 (middle top) and 200 hPa (top). The operational analyses are used as reference. Error bars show 95% confidence intervals.*

4 Summary and conclusions

This report studies the impact of different observations and background error scenarios in the analyses of soil moisture and atmospheric variables. A series of 1-month experiments at T511 spectral resolution over the US, assimilating screen level variables and SMOS T_B, were run aiming at investigating the impact of a) the type of observation assimilated in the ECMWF SEKF, compared to a soil moisture free run, b) the confidence given to SMOS T_B and c) different background error structures.

Firstly, the importance of analysing soil moisture with available observations was highlighted. The forecast of atmospheric variables, such as air temperature and air humidity, was significantly improved up to one week if screen level variables were assimilated. Also, a 1-day gain forecast in the 60% anomaly correlation was achieved with screen level data. The forecast bias of 2 m dew point temperature compared to SYNOP observations was also the minimum by using screen level variables. However, the influence of the latter in soil moisture analyses was almost negligible, at least for one month of experiments and compared to in-situ data from the SCAN and USCRN networks in US. These results points towards possible compensation mechanisms in the coupled land atmospheric model, where soil moisture is adjusted to reduce model screen level errors. On the other hand, if SMOS observations were assimilated, an improvement in the forecast of atmospheric variables, but significantly reduced compared to screen level data (especially if only SMOS data was assimilated), was obtained too compared to an open-loop run. However, for bias and RMSD, soil moisture analyses benefited from the information brought by SMOS brightness temperatures, by better matching to in-situ observations, primarily due to a reduction in bias. Nonetheless, the correlation coefficient with observations was degraded. These experiments suggest that due to the short period of the study, the correlation coefficient metric does not fully reflect the dynamical behaviour of the analyses compared to in-situ observations, and those experiments where the increments have larger variability obtain the lowest correlation with in-situ data for very dry stations with low variability of soil moisture.

Secondly, assigning twice the radiometric accuracy as the SMOS observation error had a positive impact on the temporal dynamical behaviour of the soil moisture analyses. Increasing the error of the SMOS observations produces lower increments with lower variability, which matches better the dynamic evolution of soil moisture observations in dry conditions. However the impact on the forecast of air temperature and humidity was not followed by a significant improvement, but rather a neutral impact. This result is in line with the previous one, where better scores of soil moisture were not followed by better scores for the atmosphere. Nonetheless, it is fair to claim that the observation error used for SMOS observations was underestimated, because it only accounted for the radiometric accuracy and neglected other sources of error. By giving total confidence to the SMOS observations, spurious increments were produced, which had a negative effect on both soil moisture analyses and atmospheric scores.

Thirdly, using a background error matrix as a function of soil texture, one the main parameters influencing soil moisture variability, had a positive but non significant influence on atmospheric variables. The current representation of the soil moisture background error is very crude, without any dependency on soil texture or on the depth of the soil. Introducing texture or the soil depth dependency on the background error resulted in small improvements of soil moisture analyses, air temperature and air humidity. The possible effects are likely to be observed at longer time scales. In this study, propagating the background error matrix along the assimilation window did not provide evidence of any improvement, as the size of the assimilation window and the model error introduced are too small to have a significant effect on the background error.

Therefore, the set of experiments studied in this report suggest that the combined use of a larger observation error for SMOS data with a background error dependency on soil texture in assimilation experiments, will be beneficial for soil moisture analyses and neutral-positive for the quality of atmospheric variables forecasts. The real influence of increasing the SMOS observation error and introducing a more realistic structure of the background error in the state of the soil and atmosphere, will be better understood with longer experiments and a better constrain of the atmospheric state by using a full observing system.

5 References

References

[Albergel et al. 2012] Albergel, C., P. de Rosnay, C. Gruhier, J. M. noz Sabater, S. Hasenauer, L. Isaksen, Y. Kerr, and W. Wagner, 2012 : Evaluation of remotely sensed and modelled soil moisture products using global ground-based in-situ observations. *Remote Sensing of Environment*, **18**,215–226. doi:10.1016/j.rse.2011.11.017.

[Balsamo et al. 2009] Balsamo, G., P. Viterbo, A. Beljaars, B. van den Hurk, M. Hirschi, A. Betts, and K. Scipal, 2009 : A revised hydrology for the ECMWF model: Verification from field site to terrestrial water storage and impact in the integrated forecast system. *Journal of Hydrometeorology*, **10**,623–643. doi: 10.1175/2008JHM1068.1.

[de Rosnay et al. 2012] de Rosnay, P., M. Drusch, D. Vasiljevic, G. Balsamo, C. Albergel, and L. Isaksen, 2012 : A Simplified Extended Kalman Filter for the global operational soil moisture analysis at ECMWF. *Quart J. Roy. Meteor. Soc.*, **139**,1199–1213. doi: 10.1002/qj.2023.

[Drusch et al. 2009] Drusch, M., P. de Rosnay, G. Balsamo, E. Andersson, P. Bougeault, and P. Viterbo, 2009 : Towards a Kalman filter based soil moisture analysis system for the operational ECMWF Integrated Forecast System. *Geophys. Res. Lett.*, **36**. doi:10.1029/2009GL037716, 2009.

[Drusch and Viterbo 2007] Drusch, M., and P. Viterbo, 2007 : Assimilation of screen-level variables in ECMWF's Integrated Forecast System: A study on the impact of the forecast quality and analyzed soil moisture. *Mon. Wea. Rev.*, **135**,300–314. doi - 10.1175/MWR3309.1.

[Muñoz-Sabater et al. 2014] Muñoz-Sabater, J., P. de Rosnay, C. Albergel, and L. Isaksen, 2014 : SMOS Level 3 Root Zone Soil Moisture Report and Data Assimilation Impact Report. Technical report, European Centre for Medium-Range Weather Forecasts, Reading, United Kingdom.

[Muñoz-Sabater et al. 2012] Muñoz-Sabater, J., A. Fouilloux, and P. de Rosnay, 2012 : Technical implementation of SMOS data in the ECMWF Integrated Forecasting System. *Geosc. Remote Sens. Letters*, **9**,252–256.

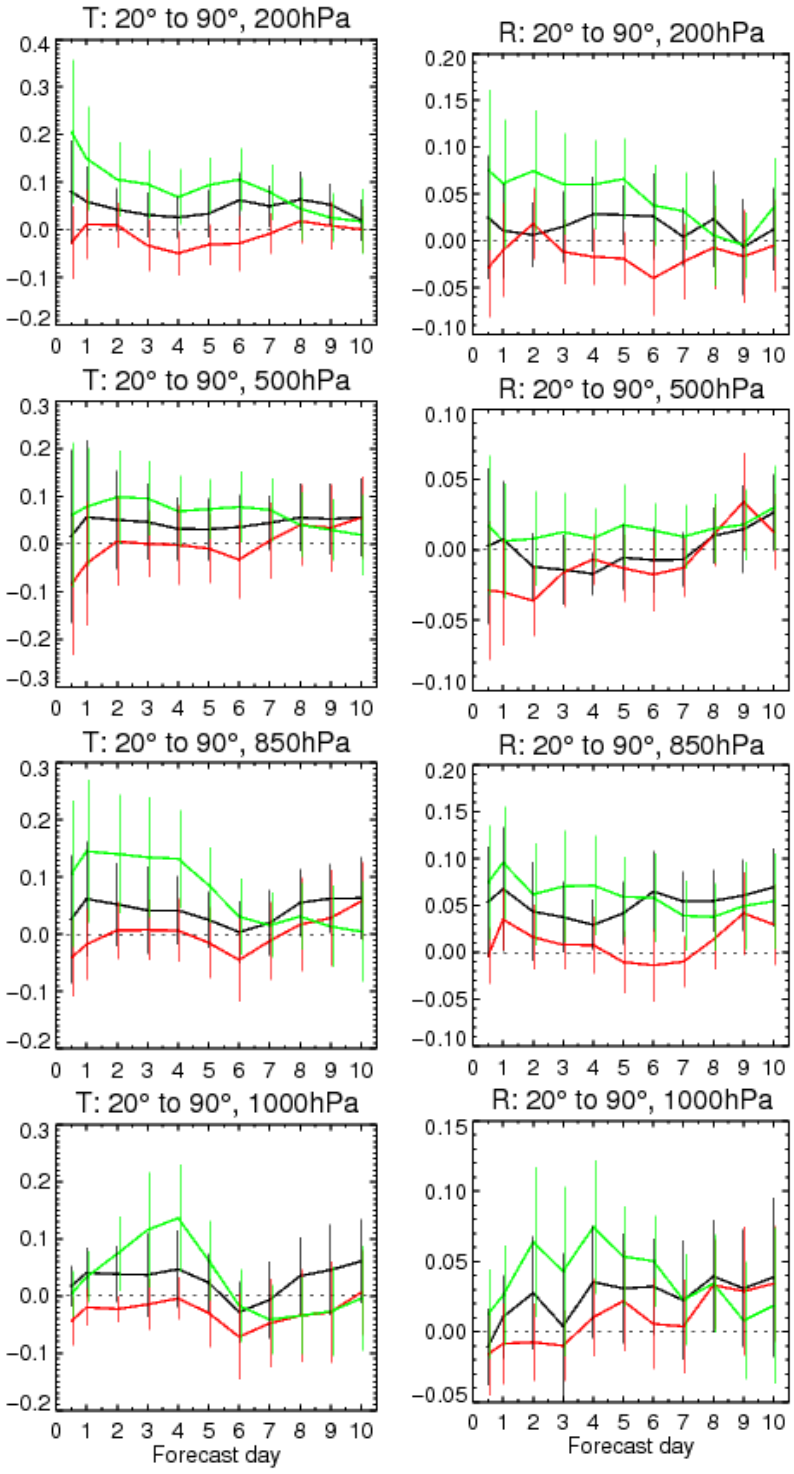

Figure 16: Air temperature (left panel) and air humidity (right panel) normalized root mean square forecast error of ***SMOS-Bprop*** *(black curve),* ***SMOS-Btext*** *(red curve) and* ***SMOS-3DB*** *(green curve) compared to the control* ***SMOS*** *experiment, as a function of the forecast lead time. Scores are shown for four different pressure levels: 1000 (bottom), 850 (middle bottom), 500 (middle top) and 200 hPa (top). The operational analyses are used as reference. Error bars show 95% confidence intervals.*

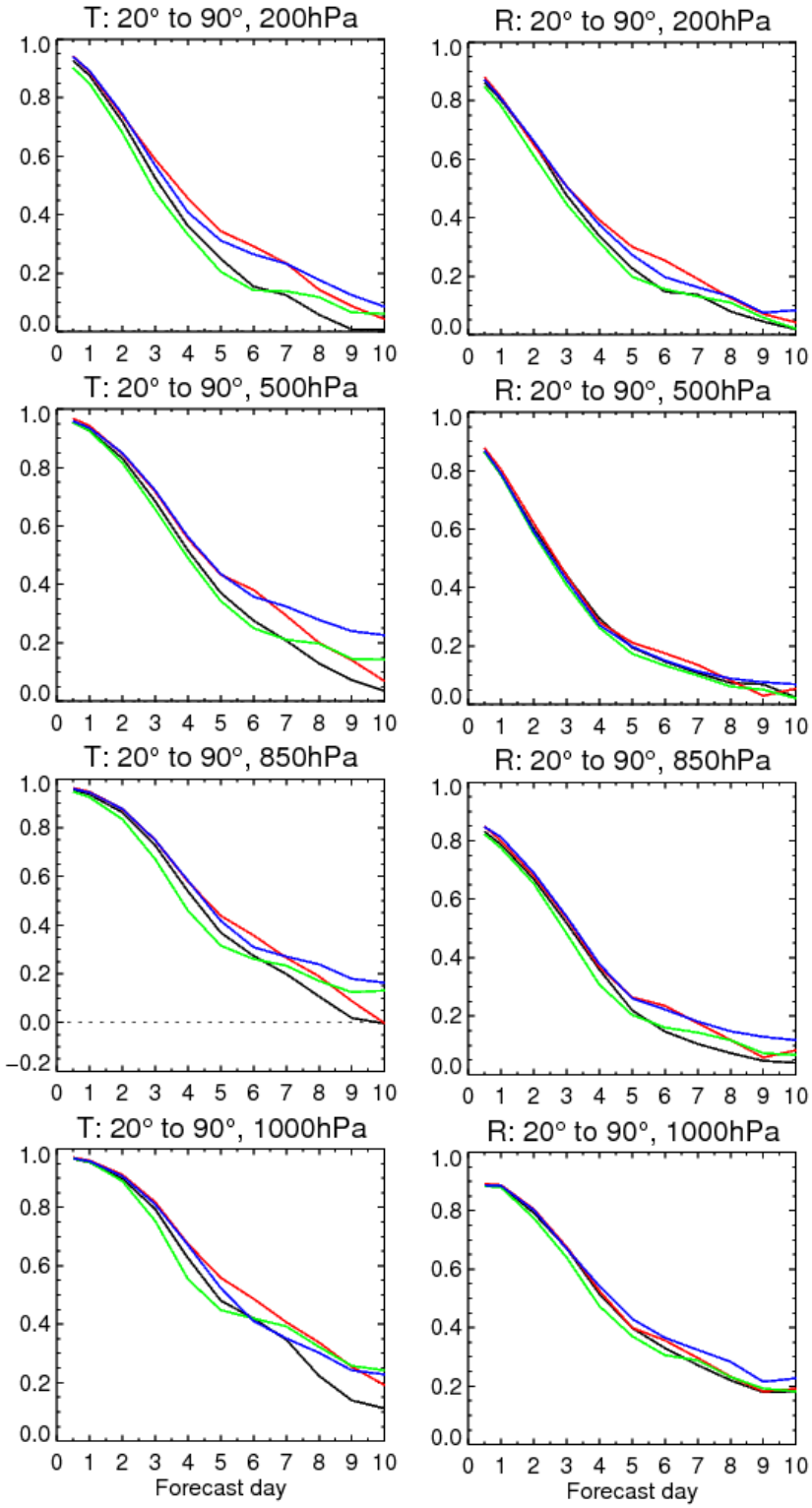

*Figure 17: Air temperature (left panel) and air humidity (right panel) anomaly correlation of **SMOS** (dark blue curve), **SMOS-Bprop** (black curve), **SMOs-Btext** (red curve) and **SMOS-3DB** (green curve) experiments, as a function of the forecast lead time. Scores are shown for four different pressure levels: 1000 (bottom), 850 (middle bottom), 500 (middle top) and 200 hPa (top). The operational analyses are used as reference. Error bars show 95% confidence intervals.*

6 Appendix

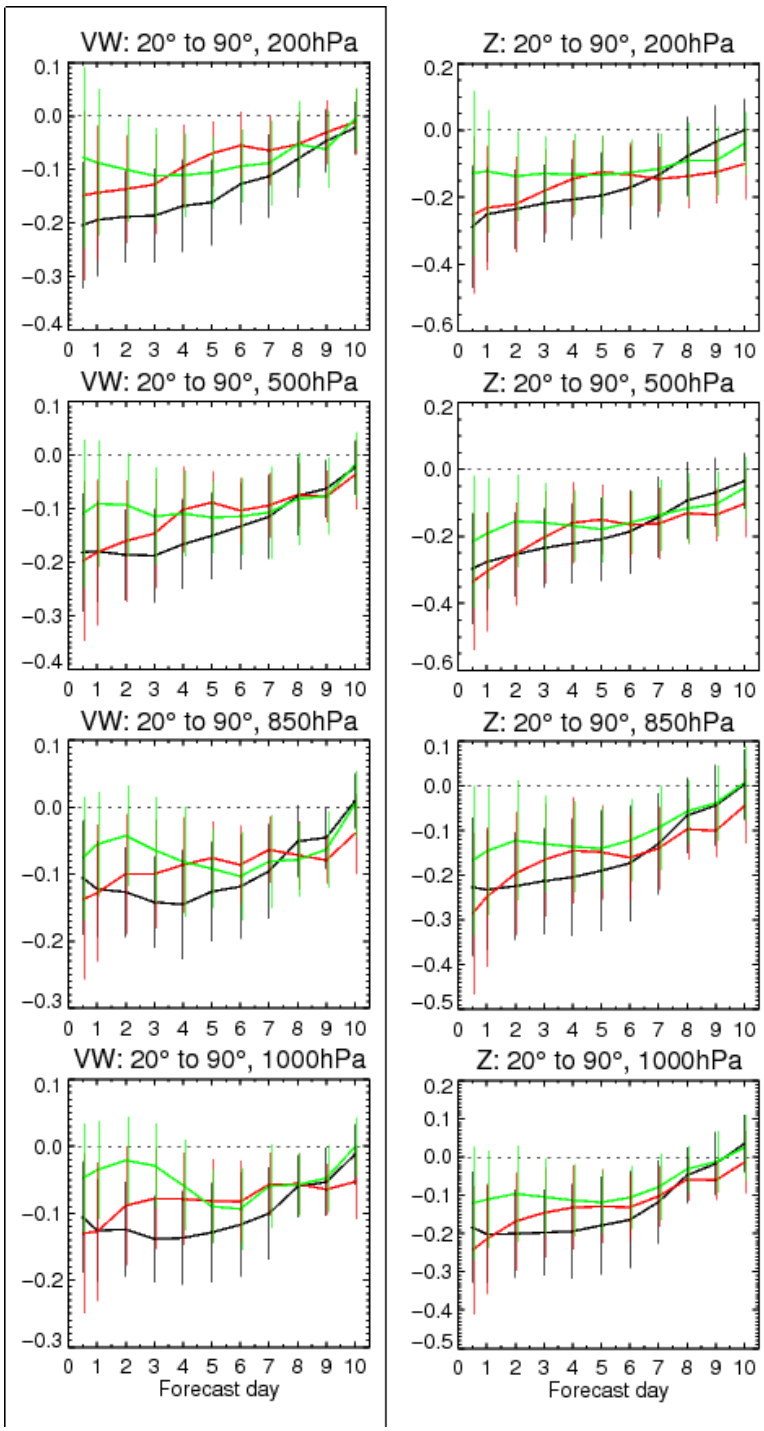

*Figure 18: Vector wind (left panel) and geopotential height (right panel) normalized root mean square forecast error of **SLV** (black curve), **SMOS** (red curve) and **SLV+SMOS** (green curve) experiments compared to the control OL experiment, as a function of the forecast lead time. Scores are shown for four different pressure levels: 1000 (bottom), 850 (middle bottom), 500 (middle top) and 200 hPa (top). The operational analyses are used as reference. Error bars show 95% confidence intervals.*

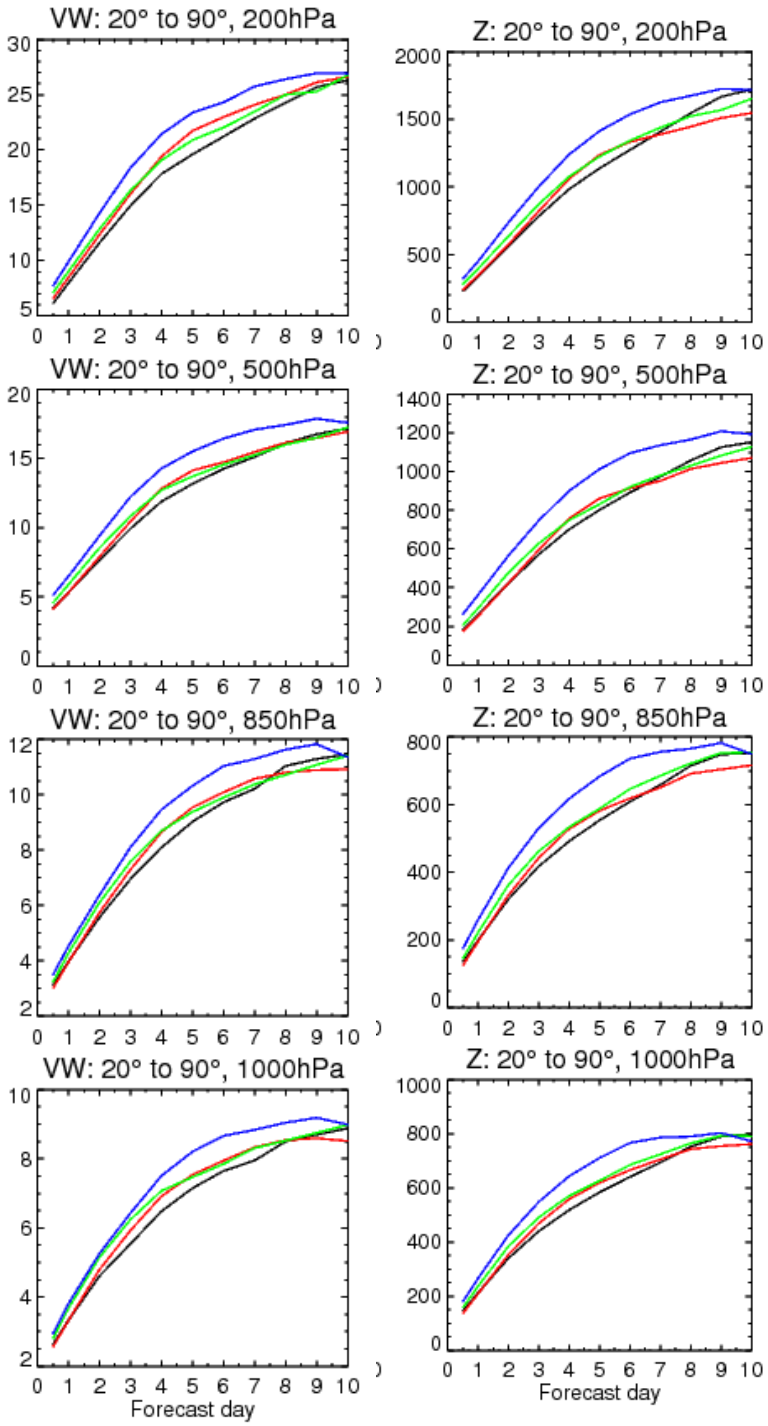

*Figure 19: Vector wind speed (left panel) and geopotential height (right panel) root mean square forecast error of the **OL** (blue curve), **SLV** (black curve), **SLV+SMOS** (green curve) and **SMOS** (red curve) experiments, as a function of the forecast lead time. Scores are shown for four different pressure levels: 1000 (bottom), 850 (middle bottom), 500 (middle top) and 200 hPa (top). The operational analyses are used as reference.*

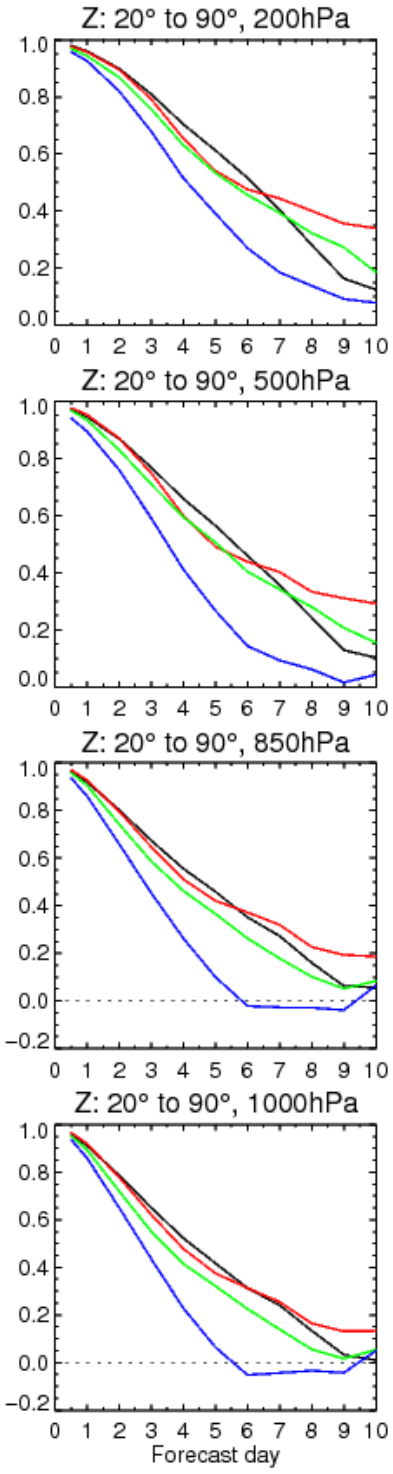

*Figure 20: Geopotential height (right panel) anomaly correlation verified against the operational analyses as a function of the forecast lead time. Blue curve is for the **OL** experiment, black curve for the **SLV** experiment, red curve for **SMOS**, and green for **SLV+SMOS** experiment. Scores are shown for four different pressure levels: 1000 (bottom), 850 (middle bottom), 500 (middle top) and 200 hPa (top).*

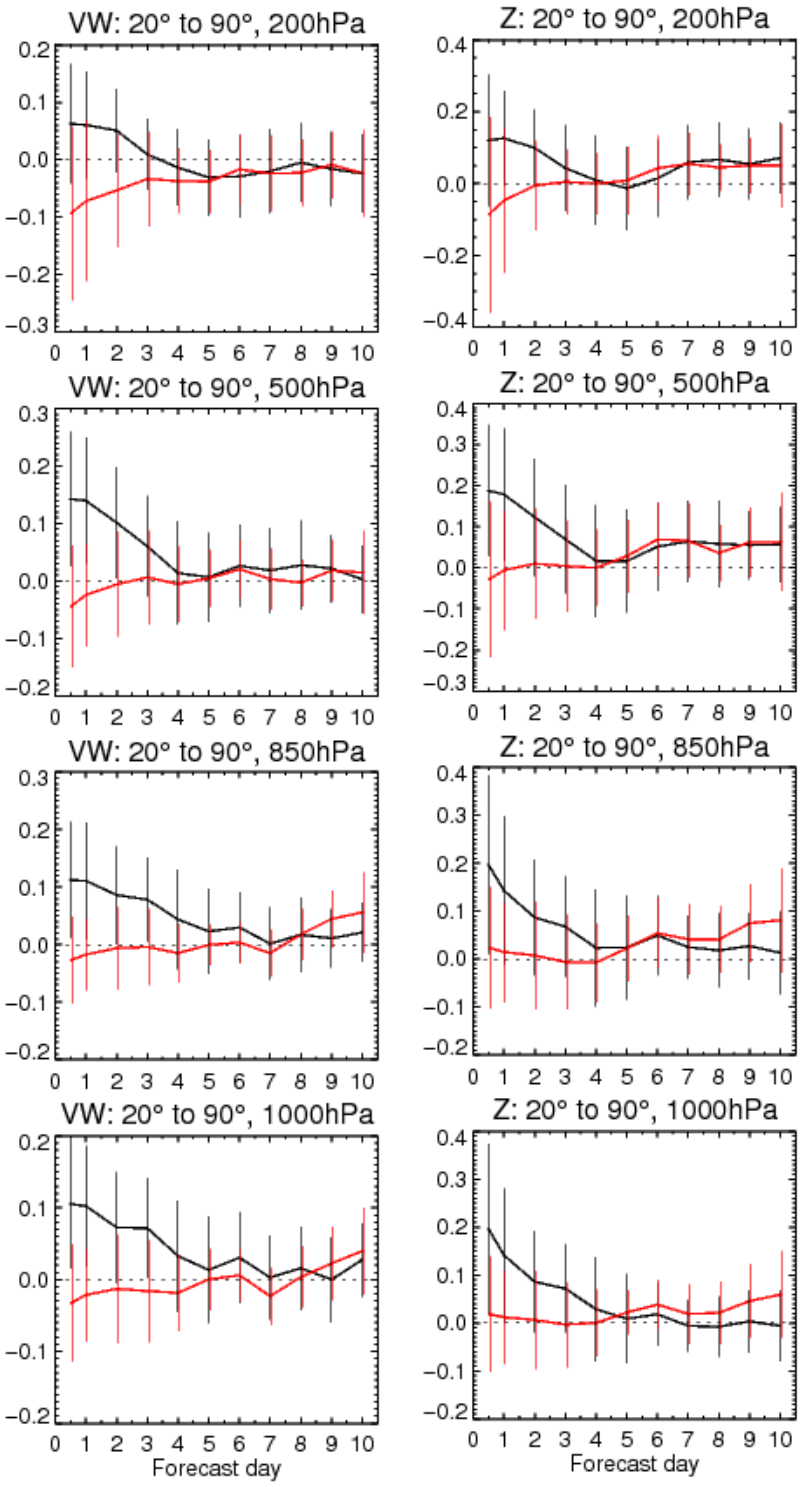

*Figure 21: Vector wind (left panel) and geopotential height (right panel) normalized root mean square forecast error of **SMOS+PI** (black curve) and **SMOS+2R** (red curve) experiments compared to the **SMOS** experiment, as a function of the forecast lead time. Scores are shown for four different pressure levels: 1000 (bottom), 850 (middle bottom), 500 (middle top) and 200 hPa (top). The operational analyses are used as reference. Error bars show 95% confidence intervals.*

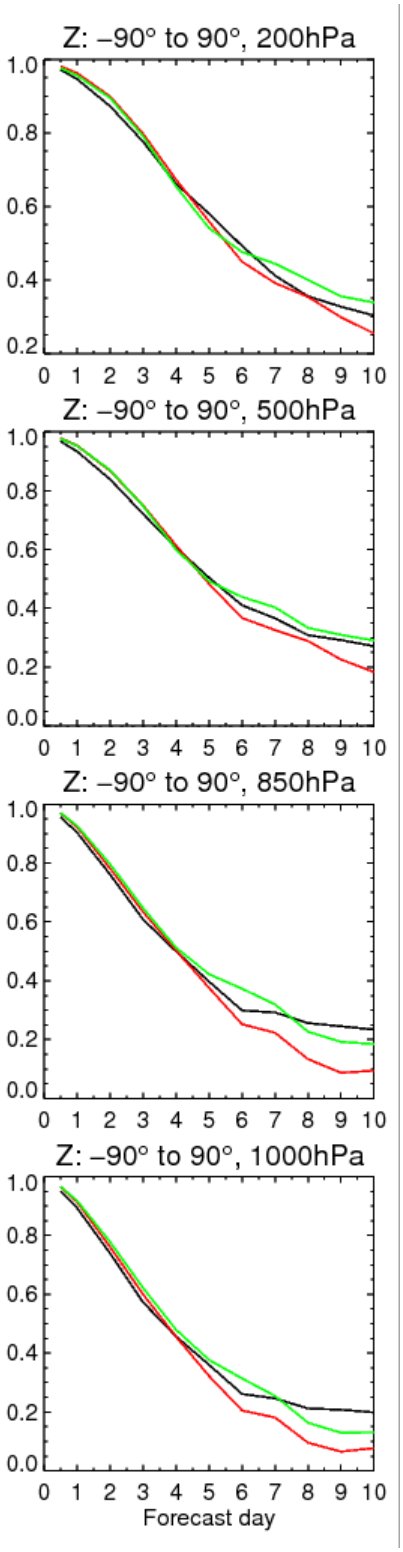

*Figure 22: Geopotential height (right panel) anomaly correlation verified against the operational analyses as a function of the forecast lead time. Black curve is for the **SMOS+PI** experiment, green for **SMOS** experiment and red curve for **SMOS+2R**. Scores are shown for four different pressure levels: 1000 (bottom), 850 (middle bottom), 500 (middle top) and 200 hPa (top).*

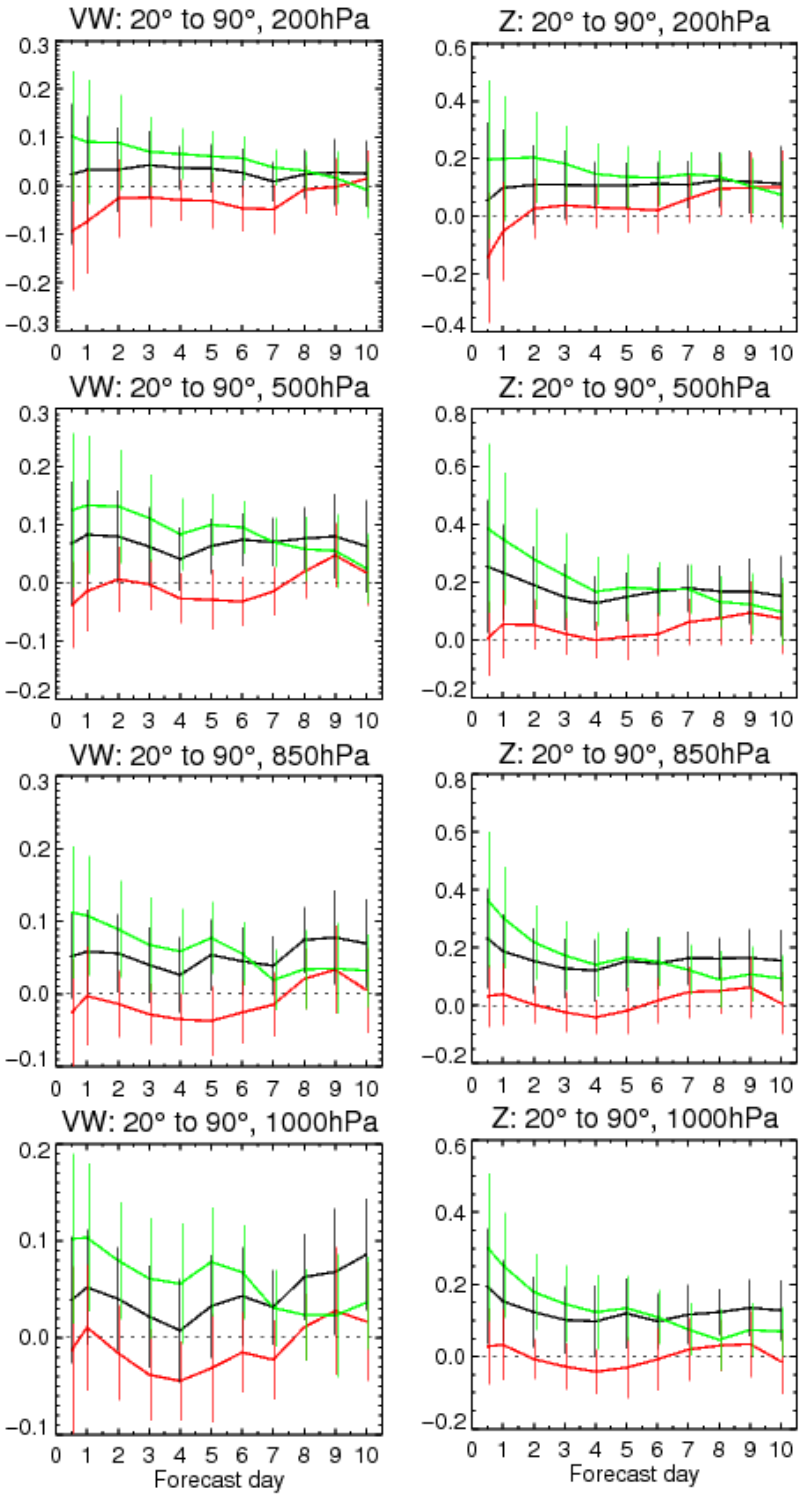

Figure 23: Vector wind (left panel) and geopotential height (right panel) normalized root mean square forecast error of ***SMOS-Bprop*** *(black curve),* ***SMOS-Btext*** *(red curve) and* ***SMOS-3DB*** *(green curve) experiments compared to the* ***SMOS*** *experiment, as a function of the forecast lead time. Scores are shown for four different pressure levels: 1000 (bottom), 850 (middle bottom), 500 (middle top) and 200 hPa (top). The operational analyses are used as reference. Error bars show 95% confidence intervals.*

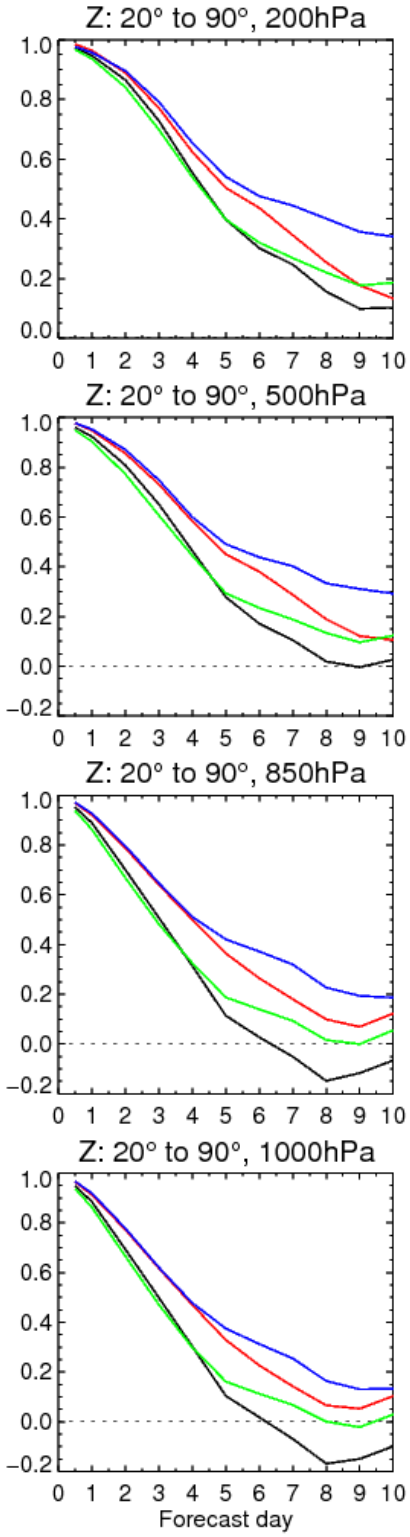

*Figure 24: Geopotential height (right panel) anomaly correlation verified against the operational analyses as a function of the forecast lead time. Dark blue curve is for the **SMOS** experiment, black for **SMOS-Bprop**, red for **SMOS-Btext** and green for **SMOS-3DB**. Scores are shown for four different pressure levels: 1000 (bottom), 850 (middle bottom), 500 (middle top) and 200 hPa (top).*

Acknowledgements

This work is funded under the ESA-ESRIN contract number 4000101703/10/NL/FF/fk. We would to thank Matthias Drusch and Susanne Mecklenburg (both ESA staff) for their involvement in this project.